Identification of Specific MicroRNAs in Neutrophils of type 2 Diabetic Mice: Overexpression of microRNA-129-2-3p Accelerates Diabetic Wound Healing

DOI:
10.2337/db18-0313

Document Version
Accepted author manuscript

Identification of specific microRNAs in neutrophils of type 2 diabetic mice: overexpression of *microRNA-129-2-3p* accelerates diabetic wound healing

Takahiro Umehara[1]*, Ryoichi Mori[2], Kimberly A. Mace[3], Takehiko Murase[1], Yuki Abe[1], Takuma Yamamoto[1], Kazuya Ikematsu[1]

[1]Division of Forensic Pathology and Science, Unit of Social Medicine, Course of Medical and Dental Sciences, Graduate School of Biomedical Sciences, Nagasaki University School of Medicine, 1-12-4 Sakamoto, Nagasaki 852-8523, Japan

[2]Department of Pathology, Nagasaki University School of Medicine and Graduate School of Biomedical Sciences, 1-12-4 Sakamoto, Nagasaki 852-8523, Japan

[3]Division of Cell Matrix Biology and Regenerative Medicine, School of Biological Sciences, Faculty of Biology, Medicine and Health, University of Manchester, Oxford Road, Manchester M13 9PT, United Kingdom

*To whom correspondence should be addressed:

Takahiro Umehara, Ph.D.

Division of Forensic Pathology and Science, Unit of Social Medicine, Course of Medical and Dental Sciences, Graduate School of Biomedical Sciences, Nagasaki University School of Medicine, 1-12-4 Sakamoto, Nagasaki 852-8523, Japan

Tel.: +81-95-819-7076

Fax: +81-95-819-7078

E-mail: umehara@nagasaki-u.ac.jp

Diabetes Publish Ahead of Print, published online December 6, 2018

Running title: miRNAs play a key role in diabetic-derived neutrophils

Abbreviations used in this paper:

BM, bone marrow

miRNA, microRNA

Casp6, *caspase 6*

Ccr1l1, *chemokine* (*C-C motif*) *receptor 1-like 1*

Ccr2, *chemokine* (*C-C motif*) *receptor 2*

Casp8, *caspase 8*

Dedd2, *death effector domain-containing DNA binding protein 2*

Db, diabetic mouse

Non-db, non-diabetic mouse

ABSTRACT

Neutrophils are involved in the first stage of acute inflammation. Following injury, they are mobilized and recruited to the injured tissue. In diabetes, wound healing is delayed and aberrant, leading to excessive recruitment and retention of neutrophils that fail to promote angiogenesis and prolong inflammation. However, the exact pathological mechanisms of diabetic-derived neutrophils in chronic inflammation remain unclear. Here, microRNA (miRNA) profiling of neutrophils from bone marrow in type 2 diabetic mice was performed using a microarray. miRNAs regulate the post-transcriptional expression of target mRNAs and are important in countering inflammation-related diseases. Our study revealed that miRNAs exhibited differential expression in diabetic-derived neutrophils compared with non-diabetic-derived neutrophils, especially *miR-129* family members. *miR-129-2-3p* directly regulated the translation of *Casp6* and *Ccr2*, which are involved in inflammatory responses and apoptosis. Furthermore, *miR-129-2-3p* overexpression at the wound site of type 2 diabetic mice accelerated wound healing. These results suggest possible involvement of *miR-129-2-3p* in diabetic-derived neutrophil dysfunction and that retention kinetics of neutrophils and chronic inflammation may be initiated via *miR-129-2-3p*-regulated genes. This study characterized changes in global miRNA expression in diabetic-derived neutrophils and systematically identified critical target genes involved in certain biological processes related to the pathology of diabetic wound healing.

Keywords: microRNA, diabetic-derived neutrophil, inflammation-related gene

INTRODUCTION

Diabetes can delay the healing of wounds and cause complications such as foot ulcers (1). Effective tissue repair requires the recruitment of immune cells from bone marrow (BM) to injured sites. In chronic wounds, the continuous influx of neutrophils and macrophages to the wound site can be maintained by stimuli such as tissue hypoxia, bacterial components, foreign bodies, and fragments of necrotic tissue (2). Chronic inflammation is predominantly characterized by excessive and prolonged infiltration of neutrophils and macrophages (3) which is frequently found in diabetic foot ulcers (4).

Skin tissue repair consists of three phases: inflammation, proliferation/migration, and maturation/resolution. Previously, we showed that the inflammatory phase is aberrant in diabetes, and the numbers of myeloid cells, including monocytes, granulocytes, and precursors, in cutaneous wounds were shown to be significantly raised on day 2 after wounding (D2W), D7W, and D10W in diabetic mice (Db) compared with those in control mice (Non-db); moreover, the recruitment and/or accumulation kinetics of these cells were altered (5). In many bacterial and autoimmune inflammatory diseases, one of the most important mechanisms of neutrophil accumulation is a delay in apoptosis due to the excessive production of neutrophil survival factors (6). As a result, inflammation is prolonged, followed by tissue damage, a feature associated with chronic inflammation in various diseases. Intrinsic factors have been shown to play an important role in aberrant myeloid cell behavior (7). Accordingly, the pathogenesis of chronic inflammation in diabetic foot ulcers may be due to intrinsic defects of diabetic-derived neutrophils. To promote diabetic skin wound healing, the mechanism behind such chronic inflammation should therefore be elucidated.

MicroRNAs (miRNAs) are small non-coding RNAs of approximately 21 to 25 nucleotides in length; they regulate post-transcriptional expression through binding to the 3′ untranslated region (3′-UTR) of target mRNAs (8, 9). Reports have described that miRNAs have an important function in several diseases (10) and wound healing, and they have been shown to comprehensively regulate a number of important biological processes within the cell (11, 12). Specifically, miRNAs play key roles in diseases such as diabetes and cancer, and chronic wounds, and are associated with cell migration, proliferation, invasion, and apoptosis. *miR-126* overexpression was shown to rescue the diabetes-induced impairment of phagocytosis of apoptotic cardiomyocytes (13). In addition, *Let-7b* was revealed to inhibit keratinocyte migration in cutaneous wound healing (14). Moreover, reports have described that the topical application of miR-132 mimic mixed with pluronic F-127 gel in chronic wounds promoted re-epithelialization (15), and that miR-27b rescued impaired bone marrow-derived angiogenic cell function and improved wound healing in type 2 diabetic mice (16). miR-191 modulates cellular migration and angiogenesis to delay the tissue repair process (17). We also reported that miR-142 is required for the clearance of *Staphylococcus aureus* at skin wound sites (18). Against this background, functional analysis of miRNAs in the complex process of wound healing could confer great benefits for manipulation in the clinic, but the exact molecular mechanisms involved in diabetic skin wound healing leading to chronic inflammation remain largely unknown.

We hypothesized that miRNAs might be involved in the functional regulation of diabetic-derived neutrophils in chronic inflammation. To clarify the molecular mechanism of inflammatory control in diabetic-derived neutrophils, we screened for changes of miRNA expression in diabetic-derived neutrophils using microarrays. Next,

we evaluated the expression of specific miRNA and its target genes in diabetic-derived neutrophils and/or skin wounds. Finally, we examined the involvement of this miRNA in diabetic skin wound healing.

MATERIALS AND METHODS

Mouse wounding model

The Animal Care Committee of Nagasaki University approved the protocol for this study (approval number: 1407101159). BKS.Cg-*Dock7*^{m} +/+ *Lepr*^{db}/J (*Lepr*$^{db/db}$ and *Lepr*$^{db/+}$) mice (5 weeks old) were purchased from Charles River Laboratories (Yokohama, Japan). They were housed under a 12/12-h light/dark cycle (light on: 07:00, off: 19:00) at constant temperature and humidity and allowed free access to food and water. Male mice were used between 8 and 12 weeks of age and were age-matched to controls. To eliminate the effect of hormonal action related to sexual maturation on skin wound healing, we used only male mice. Full-thickness excisional dorsal wounds (4 mm) were made by a biopsy punch. Wounds were harvested, including a 2-mm margin of skin.

Mature miRNA purification for microarray analysis

Bone marrow (BM) was flushed from femurs and tibiae. Neutrophils from the pooled BM of three db or three non-db mice were isolated using a neutrophil isolation kit (Miltenyi Biotec Inc., Bergisch Gladbach, Germany), and miRNA was purified from neutrophils using a microRNA isolation kit, Mouse Ago2 (Wako, Osaka, Japan) for microarray analysis.

Microarray analysis

Microarray analysis was performed on a total of eight pools (four pools of three db BM samples and four pools of three non-db BM samples) using SurePrint G3 Mouse miRNA microarray, in accordance with the manufacturer's instructions (Agilent Technologies, Tokyo, Japan). Bioinformatic analyses were performed using GeneSpring v13 (Agilent Technologies). The data discussed in this publication have been deposited in NCBI's Gene Expression Omnibus and are accessible through GEO Series accession number GSE100577.

Isolation of neutrophils, macrophages, T cells, and B cells

Neutrophils from BM of six non-db mice were isolated using a neutrophil isolation kit (Miltenyi Biotec Inc.). Macrophages, T cells, and B cells from BM of six non-db mice were isolated with a Microbead Kit (Miltenyi Biotec Inc.), in accordance with the manufacturer's instructions. Cells were incubated with anti-CD11b Ab, anti-CD5 Ab, and anti-CD19 Ab to isolate macrophages, T cells, and B cells, respectively.

RNA isolation for real-time quantitative PCR

Neutrophils from BM and skin wounds of six db and six non-db mice were isolated using a neutrophil isolation kit and Anti-Ly-6G Microbead kit (Miltenyi Biotec). Wound skin from D2W and D3W was harvested by a biopsy punch (6 mm). It was then dissolved in QIAzol Lysis Reagent (QIAGEN, Germantown, MD, USA). Total RNA, including miRNA, was extracted using miRNeasy Mini kit and RNeasy Mini Kit (QIAGEN), in accordance with the manufacturer's instructions. Total RNA was quantified using NanoDrop™ 2000 Spectrophotometers (Thermo Fisher Scientific,

Waltham, MA, USA). RNA samples were stored at −80°C until use.

cDNA synthesis for mRNA and microRNA, and quantitative real-time PCR

Total RNA (850 ng) was utilized as a template and complementary DNA (cDNA) was synthesized using Prime-Script® RT Reagent Kit for mRNA expression analysis (Takara Bio, Kusatsu, Japan), in accordance with the manufacturer's instructions. Quantitative real-time PCR (qRT-PCR) was performed in a 10-μL reaction system using SYBR Premix Ex Taq (Takara Bio) and a Thermal Cycler Dice Real Time System (Takara Bio). The contents of the amplification mix and thermal cycling conditions were set in accordance with the manufacturer's instructions. Primers [*Caspase 6* (*Casp6*), *Chemokine* (*C-C motif*) *receptor 1-like 1* (*Ccr1l1*), *Chemokine* (*C-C motif*) *receptor 2* (*Ccr2*), *Caspase 8* (*Casp8*), *Death effector domain-containing DNA binding protein 2* (*Dedd2*), glyceraldehyde-3-phosphate dehydrogenase (*Gapdh*), *CCR2*, *DEDD2* and *GAPDH*] were purchased from Takara Bio Inc. TaqMan® Gene Expression Assay (Thermo Fisher Scientific) for *CASP6* was performed in accordance with the manufacturer's instructions.

Total RNA (10 ng) was utilized as a template and cDNA synthesis and qRT-PCR were performed using miRCURY LNA™ Universal RT microRNA PCR and LNA™ PCR primer set for miRNA expression analysis (EXIQON, Vedbaek, Denmark). Primers (*mmu-* (*hsa-*) *miR-129-2-3p* and *5S rRNA*) were purchased from EXIQON. The relative quantification of mRNA transcripts and miRNA was performed using the ΔΔCt method (19).

Synthesis of DNA, miRNA mimic, and mutation

Putative target genes of *miR-129-2-3p* were predicted using GeneSpring (Agilent Technologies). DNA synthesis of *Casp6*, *Ccr2* and *Dedd2* was performed by Hokkaido System Science Co., Ltd. (Sapporo, Japan). Luciferase reporter plasmids were constructed to confirm the regulation of target genes by *miR-129-2-3p*. *miR-129-2-3p* mimic (chemically synthesized double-stranded mature *miR-129-2-3p*) and mutation as a negative control were chemically synthesized by GeneDesign, Inc. (Ibaraki, Osaka, Japan).

Cell culture and reagents

3T3 cells were cultured for luciferase reporter assay in Dulbecco's modified Eagle's medium (DMEM) (Wako) with high glucose, L-glutamine, 10% FBS, and 1% penicillin–streptomycin. These cells were then harvested, seeded onto a 96-well plate at about 3.0×10^4 cells per well in DMEM (Wako) with 10% FBS without 1% penicillin–streptomycin, and cultured for 24 h. Subsequently, these cells were washed with Opti-MEM (Thermo Fisher Scientific), supplemented with 100 μL of Opti-MEM in each well, and incubated at 37 °C prior to transfection.

Transfection and luciferase reporter assay

The 3′-UTRs of *miR-129-2-3p* targets were predicted using TargetScan (http://www.targetscan.org/vert_71/) and microT-CDS in DIANA TOOLS (http://diana.imis.athena-innovation.gr/DianaTools/index.php?r=microT_CDS/index). Vectors were constructed with pmirGLO Dual-Luciferase miRNA Target Expression Vector (Promega Corp., Madison, WI, USA), in accordance with the manufacturer's instructions. Primers consisting of the 3′-UTRs of predicted *miR-129-2-3p* target

sequences and appropriate restriction sites were synthesized, annealed, and cloned downstream of the firefly luciferase reporter (*luc2*) gene in pmirGLO. Sequences were as follows:

Casp6 sense 5′-aaacTGTTGGACGTGGTGGAAGGGCTAt-3′

Casp6 antisense 5′-ctagaTAGCCCTTCCACCACGTCCAACAgttt-3′

Ccr2 sense 5′-aaacAGTGATTAGACTAAAAATAATAAGGGCTt-3′

Ccr2 antisense 5′-ctagaAGCCCTTATTATTTTTAGTCTAATCACTgttt-3′

Dedd2 sense 5′-aaacCTGCCCCACACACTTTAGCCTAAGGGCTAt-3′

Dedd2 antisense 5′-ctagaTAGCCCTTAGGCTAAAGTGTGTGGGGCAGgttt-3′.

Upper- and lower-case letters indicate the 3′-UTR and restriction sites (PmeI and XbaI), respectively.

Sequences *of miR-129-2-3p* mimic and mutation of seed sequence as a negative control were as follows:

miR-129-2-3p mimic 5′-AAGCCCUUACCCCAAAAAGCAU-3′

miR-129-2-3p mutation 5′-AAUCCCCUACCCCAAAAAGCAU-3′.

3T3 cells (3.0×10^4 cells/100 μl) were cotransfected with the *miR-129-2-3p* mimic or mutation and a reporter plasmid containing the 3′-UTR of *Casp6*, *Ccr2*, and *Dedd2*. The *miR-129-2-3p* mimic and mutation were added at a final concentration of 40 nM with Lipofectamine3000 (Invitrogen). At 48 h after transfection, luciferase activity was assessed using a Dual-Glo Luciferase Assay System (Promega Corp.), in accordance with the manufacturer's instructions.

Induction of neutrophil differentiation

The HL-60 human promyelocyte cell line (RBRC-RCB0041) was provided by RIKEN BRC through the National Bio-Resource Project of MEXT, Japan. The HL-60 cells were cultured in RPMI-1640 medium (Thermo Fisher Scientific) with 10% FBS, and 1% penicillin–streptomycin. Neutrophil differentiation was induced by exposing HL-60 cells to 1.3% DMSO (Wako) for 5 days. At 3 days after exposure to 1.3% DMSO, HL-60 cells were transfected with *miR-129-2-3p* mimic or mutation at a final concentration of 70 nM using Lipofectamine3000 (Thermo Fisher Scientific) in Opti-MEM (Thermo Fisher Scientific) with 1.3% DMSO. Two days after transfection, cells and conditioned media were harvested and applied to target gene expression analysis.

Immunohistochemistry

Harvested tissues (D0W–D3W) were fixed in 4% paraformaldehyde (PFA) overnight and embedded in paraffin. All specimens were cut into 4-μm-thick sections. IHC was performed with anti-Ly-6G (α-Ly-6G, neutrophil marker) as a primary antibody in accordance with manufacturer's protocol (Abcam, Cambridge, UK). Rat anti-mouse Ly-6G was purchased from Novus Biologicals (Littleton, CO, USA). Samples were incubated with Histofine® Simple Stain TM Mouse MAX PO (Rat) (Nichirei Bioscience Inc., Tokyo, Japan) for 1 h at room temperature. The Histofine® DAB-3S kit (Nichirei Bioscience Inc.) was used as a color developer. Hematoxylin was used as a nuclear counterstain. Observations were made via Aperio AT Turbo (Leica Microsystems, Tokyo, Japan).

Double-label fluorescent IHC (fIHC) was performed with CASP6 (Abcam [Table 1], Dilution: 1:500) or CCR2 (Abcam: ab203128, Dilution: 1:100), and anti-Ly-6G

(α-Ly-6G, neutrophil marker, Dilution: 1:200) as primary antibodies in accordance with IHC and immunofluorescence (IF) protocols (Abcam). Goat anti-rabbit IgG (H+L), Alexa Fluor® 488 conjugated (α-rabbit 488), and Alexa Fluor® 594 conjugated (α-rat 594) secondary antibodies (Dilution: 1:500) were purchased from Life Technologies. Observations were made via confocal microscopy (C2+ system; Nikon Corp., Tokyo, Japan). NIS-Elements C software version 4.13 (Nikon Corp.) and IMARIS 7.6.5 (BITPLANE, Zurich, Switzerland) was used for data analysis.

Morphometric analysis of neutrophils

For each tissue image of 3–5 wounds in wound area for IHC, binarization was performed. Ratios of the neutrophil-positive area relative to the wound area were calculated.

***In situ* hybridization**

In situ hybridization (ISH) was performed using microRNA ISH buffer set and miRCURY LNA Detection 5′- and 3′-DIG labeled probes (QIAGEN), in accordance with the manufacturer's instructions. In brief, 4% PFA perfusion-fixed tissues were embedded in paraffin. Six-micrometer-thick sections were deparaffinized and incubated with Proteinase K solution (DAKO, Glostrup, Denmark) for 10 min at 37°C. After washing in PBS, sections were dehydrated. Hybridization was performed using 20 nM miRNA probe in microRNA ISH buffer (QIAGEN) at 50°C for 3 h. Sections were rinsed in 5× SSC at 50°C for 5 min, twice with 1× SSC at 50°C for 5 min, twice with 0.2× SSC at 50°C for 5 min, and with 0.2× SSC at room temperature for 5 min. Sections were treated with blocking solution (Nacalai Tesque Inc., Kyoto, Japan) for 15 min at

room temperature and were then incubated with anti-DIG Ab (1:800) (Roche Diagnostics GmbH, Mannheim, Germany) in blocking solution (Nacalai Tesque Inc.) overnight at 4°C. Sections were developed using NTB/BCIP (Roche Diagnostics GmbH) at 30°C. Observations were made via Aperio AT Turbo (Leica Microsystems) and confocal microscopy (C2+ system). NIS-Elements C software version 4.13 was used for data analysis.

Total protein extraction and western immunoblot analysis

Skin tissue was homogenized using a TissueLyzer II (QIAGEN). T-PER Reagent (Thermo Fisher Scientific), consisting of proteinase and dephosphorylation inhibitor (Thermo Fisher Scientific), was then added. Debris was removed from the supernatant using an Ultrafree-MC 0.45-mm filter (Merck Millipore, Darmstadt, Germany). Filtered protein samples were quantified using a Direct Detect Spectrometer (Merck Millipore), separated on 4% to 12% NuPAGE Novex Bis-Tris gels (Thermo Fisher Scientific), transferred to polyvinylidene difluoride (PVDF) membranes, and blotted in accordance with standard protocols (antibody details are listed in Table 1). Protein bands were visualized using ImmunoStar® LD (Wako), and band intensity was calculated using Multi Gauge version 3.X (Fujifilm, Tokyo, Japan).

Skin wound healing studies using *miR-129-2-3p* mimic and mutation

For *in vivo* experiments, *miR-129-2-3p* mimic or mutation as a negative control [10 μmol/L in 50 μL of 30% Pluronic F-127 gel (Sigma Aldrich, St. Louis, MO)] was topically applied immediately after wounding. Thereafter, the proportion of wound area on each day after wounding relative to the initial wound area was measured using

Adobe Photoshop CC.

Statistical analysis

Data are shown as means ± SD. The statistical significance of differences between means was assessed by Mann–Whitney *U* test, one-way ANOVA, followed by Tukey's multiple comparison test and two-way ANOVA, followed by Bonferroni post-tests to compare replicate means (GraphPad Software, San Diego, CA, USA). A p-value < 0.05 was considered significant.

RESULTS

miRNA expression is altered in diabetic-derived neutrophils

Microarray analysis showed that the expression levels of 22 miRNAs in diabetic-derived neutrophils were more than double those in non-diabetic-derived neutrophils (Supplementary Fig. 1A), while those of 80 miRNAs were decreased to less than half in fold change analysis (Supplementary Fig. 1B), although statistical analysis was not performed on this.

In turn, we performed a moderated *t*-test (cut-off<0.05) and Storey with bootstrapping for microarray data using GeneSpring. Microarray analysis showed that the expression levels of 10 miRNAs in diabetic-derived neutrophils were significantly decreased compared with those in non-diabetic-derived neutrophils (Fig. 1A, Table 2). We focused here on *miR-129-2-3p* because the microarray data indicated that the signal values of db in miRNAs were too low, with the exception of *miR-129-2-3p* (Fig. 1B), and that *miR-129-2-3p* in diabetic-derived neutrophils was downregulated to less than one-third of the level in non-diabetic-derived neutrophils (Table 2).

qRT-PCR using the SYBR Green I assay showed that the expression of *miR-129-2-3p* in diabetic-derived neutrophils was significantly decreased [expression level (mean ± SD): Non-db: 6.3 ± 4.4, Db: 0.70 ± 0.35, p=0.0079] (Fig. 1C).

miR-129-2-3p is mainly expressed in neutrophils

To examine the cellular expression of *miR-129-2-3p*, we isolated neutrophils, macrophages, B cells, and T cells from BM and spleen in non-db using Microbead Kit, and examined the expression of *miR-129-2-3p* using qRT-PCR. Its expression was significantly increased in neutrophils compared with that in other cells in BM (Fig. 1D), and increased in neutrophils and macrophages compared with the levels in B cells and T cells in the spleen (Supplementary Fig. 2). Accordingly, this suggests that *miR-129-2-3p* is related to inflammation, especially early inflammation.

mRNAs are predicted to be target genes of differentially expressed miRNAs in microarray

More than 800 mRNAs were predicted to be targets of the miRNAs shown in Table 2 that were significantly differentially expressed in diabetic-derived neutrophils (Supplementary Fig 3). We thus performed Gene Ontology (GO) and pathway analyses using GeneSpring to survey them. The results showed that candidate target mRNAs for *miR-129-2-3p* were associated with many biological processes and pathways, including inflammatory response, apoptosis, chemotaxis, phagocytosis, endocytosis, and chemokine signaling. Accordingly, a number of biological processes may be defective in diabetic-derived neutrophils (Table 3).

Predicted target mRNAs show an inverse correlation with *miR-129-2-3p* expression

GO and pathway analyses showed that *caspase 6* (*Casp6*), *chemokine* (*C-C motif*) *receptor 1-like 1* (*Ccr1l1*), and *chemokine* (*C-C motif*) *receptor 2* (*Ccr2*) are associated with inflammatory responses, and *caspase 8* (*Casp8*) and *death effector domain-containing DNA binding protein 2* (*Dedd2*) are also involved in apoptosis. These genes were expressed at high levels in diabetic-derived neutrophils compared with their levels in non-diabetic-derived neutrophils, as confirmed by qRT-PCR [expression levels (mean ± SD): *Casp6*: Non-db: 0.76 ± 0.13, Db: 0.97 ± 0.079, p=0.0042; *Ccr1l1*: Non-db: 0.33 ± 0.22, Db: 1.0 ± 0.23, p=0.0023; *Ccr2*: Non-db: 0.37 ± 0.061, Db: 1.4 ± 0.33, p=0.0022; *Casp8*: Non-db: 0.88 ± 0.074, Db: 1.2 ± 0.16, p=0.0077; and *Dedd2*: Non-db: 0.60 ± 0.13, Db: 0.89 ± 0.086, p=0.0043] (Fig. 2A–E). These results support the prediction that these mRNAs are targets of *miR-129-2-3p*, as the expression of these genes was significantly increased, whereas the expression of *miR-129-2-3p* was significantly decreased, in diabetic-derived neutrophils.

miR-129-2-3p* directly regulates *Casp6*, *Ccr2*, and *Dedd2* translation *in vitro

To verify that the mRNAs that we identified were targets of *miR-129-2-3p*, we tested each in a luciferase reporter assay. *miR-129-2-3p* is predicted to bind with high affinity to *Casp6*, *Ccr2*, and *Dedd2* 3′-UTRs (Fig. 3A). In this assay, a decrease in luciferase activity indicates the binding of the miRNA mimic to the 3′-UTR of the target sequence. Luciferase reporter assays showed that the *miR-129-2-3p* mimic could effectively inhibit the expression of *Casp6* (Control: 1.0 ± 0.15, mimic: 0.61 ± 0.13, p=0.0022), *Ccr2* (Control: 1.0 ± 0.083, mimic: 0.73 ± 0.10, p=0.029), and *Dedd2* (Control: 1.0 ±

0.13, mimic: 0.69 ± 0.089, p=0.0079) (Fig. 3B-D); thus, we concluded that *miR-129-2-3p* directly regulates the expression of *Casp6*, *Ccr2*, and *Dedd2 in vitro*.

miR-129-2-3p directly regulates _CASP6_ and _DEDD2_ translation in HL-60 cells

To determine whether *CASP6*, *CCR2*, and *DEDD2* can be direct targets of *miR-129-2-3p*, we used HL-60 cells, which are human neutrophil-like cells. qRT-PCR showed that the expression of *CASP6* and *DEDD2* in HL-60 cells transfected with *miR-129-2-3p* mimic was significantly decreased compared with that in those transfected with mutant *miR-129-2-3p* [expression levels (mean ± SD): *CASP6*: mutant: 1.0 ± 0.23, mimic: 0.71 ± 0.050, p=0.029; *DEDD2*: mutant: 1.1 ± 0.30, mimic: 0.57 ± 0.12, p=0.017] (Fig. 3E–F), although the expression of *CCR2* could not be detected in HL-60 cell. These results suggested that these target genes might be directly regulated by *miR-129-2-3p* in HL-60 cells. Therefore, further investigation of these genes is necessary using human diabetic wound samples in order to apply the obtained findings to diabetes in humans.

Wound neutrophils are increased in db D2W, and _miR-129-2-3p_ is predominantly expressed in wound neutrophils

To investigate the proportion of neutrophils among cells present at the early stage of inflammation (D1W-D2W), we performed IHC at wound sites in db and non-db mice. IHC for neutrophils showed a stronger signal in db D2W compared with non-db (Fig. 4A). Moreover, we calculated ratios of neutrophil-positive area relative to the wound area at D1W and D2W. The results showed that there were significantly more neutrophils present in D2W of db [signal level (mean ± SD): Non-db: 4.5 ± 0.97, Db:

9.01 ± 1.3, *p*=0.029] (Fig. 4B).

To determine which cells express *miR-129-2-3p* during the early stage of inflammation, we performed ISH in D1W of non-db. ISH showed that *miR-129-2-3p* was predominantly expressed in wound-infiltrating neutrophils in D1W (Fig. 4C).

miR-129-2-3p is insufficiently activated in diabetic-derived neutrophils

To elucidate whether *miR-129-2-3p* and its target genes are involved in prolonged inflammation and delayed wound healing, we examined the expression of these genes at the skin wound site in D2W.

The expression of *miR-129-2-3p* did not show a significant difference between non-db and db at D2W (data not shown), upon isolating the neutrophils from non-db and db wound skin at day 2 after wounding using Anti-Ly-6G Microbead kit (Miltenyi Biotec) and examining the expression of *miR-129-2-3p* in equal numbers of neutrophils from the two groups. The expression of *miR-129-2-3p* in neutrophils from db D2W was significantly decreased compared with that in non-db [expression level (mean ± SD): Non-db: 7.0 ± 2.1, Db: 2.2 ± 0.69, *p*=0.016] (Fig. 4D). The expression of the *miR-129-2-3p* target gene, *Casp6* in db D2W was significantly increased compared with that in non-db [expression level (mean ± SD): Non-db: 2.1 ± 0.24, Db: 2.6 ± 0.082, *p*=0.0029] (Fig. 4E). Similarly, the expression of *Ccr2* in db D2W was significantly increased compared with the level in non-db [expression level (mean ± SD): Non-db: 4.4 ± 0.55, Db: 5.7 ± 0.34, *p*=0.0025] (Fig. 4F). In contrast, the expression of *Dedd2* in db D2W was significantly decreased compared with the level in non-db [expression level (mean ± SD): Non-db: 0.85 ± 0.11, Db: 0.39 ± 0.12, *p*=0.0022] (Fig. 4G). The data clearly show that, in neutrophils, *Dedd2* is a target of *miR-129-2-3p*; however, it may be

that, at this time point during wound healing, some other factors such as other miRNAs inhibit *Dedd2*, and that this mechanism is even more effective in diabetic wounds. Additionally, the expression of *Casp8* in db D2W was significantly increased compared with the level in non-db (Supplementary Fig 4A).

The expression of cleaved CASP6 in D2W did not show significant change between non-db and db although the number of neutrophils at D2W in db was significantly higher than in non-db (Fig. 4H). This result suggests that apoptosis of cells present in the wound site might be delayed.

To determine whether neutrophils express CASP6 and CCR2 during the early stage of inflammation, we performed fIHC in db D2W. fIHC showed that CASP6 and CCR2 was predominantly expressed in neutrophils (Supplementary Fig 4B).

Based on the results of IHC (Fig. 4A–B) and our previous report (5), the expression of *miR-129-2-3p* showed a significant decrease in db, although the number of neutrophils at D2W in db was significantly higher than in non-db. In addition, *Casp6* and *Ccr2* tended to be overexpressed in db D2W, and *miR-129-2-3p*, CASP6 and CCR2 was predominantly expressed in wound-infiltrating neutrophils (Fig. 4C, Supplementary Fig 4B). These results suggested that *miR-129-2-3p* was insufficiently activated in diabetic-derived neutrophils in D2W.

Overexpression of *miR-129-2-3p* in skin wound site of type 2 diabetic mice accelerates wound healing

We previously reported the usefulness of AS ODN using pluronic F-127 gel in skin wound (20). Therefore, it is useful to use a gel to verify the role of molecules in wound healing.

First, to clarify the pathophysiological role of *miR-129-2-3p* in skin wound healing, we made a wound in the dorsal skin of db and topically applied *miR-129-2-3p* mimic or mutant negative control mixed with pluronic F-127 gel immediately after wounding. Wound closure was significantly accelerated in *miR-129-2-3p* mimic-treated compared with *miR-129-2-3p* mutant control-treated wounds from D7W to D21W in db mice [Wound area (%) (mean ± SD): day 7: mutation: 130.5 ± 18.2, mimic: 101.4 ± 18.1, $p < 0.05$, day 10: mutation: 132.2 ± 38.3, mimic: 96.6 ± 16.3, $p < 0.01$, day 14: mutation: 115.2 ± 25.9, mimic: 70.4 ± 29.0, $p < 0.001$, day 21: mutation: 36.8 ± 14.4, mimic: 11.0 ± 9.5, $p < 0.05$] (Fig. 5A and 5B), although there was no apparent effect in non-db mice [Wound area (%) (mean ± SD): day 7: Non-db: 38.2 ± 25.7, Db: 130.5 ± 18.2, $p < 0.001$, day 10: Non-db: 10.1 ± 1.9, Db: 132.2 ± 38.3, $p < 0.001$, day 14: Non-db: 2.0 ± 0.86, Db: 115.2 ± 25.9, $p < 0.001$].

Next, to investigate the proportion of neutrophils among cells present at D3W, we performed IHC at the wound site in day 3 from application of mimic or mutation immediately after wounding of db. IHC for neutrophils showed a positive signal in *miR-129-2-3p* mutant control-treated wounds (Fig. 5C). Moreover, we examined the relative neutrophil-positive area in D3W and found a reduced signal in *miR-129-2-3p* mimic-treated D3W compared with that in *miR-129-2-3p* mutant control-treated [signal level (mean ± SD): mutation: 8.9 ± 2.8, mimic: 5.1 ± 1.1, p=0.057] (Fig. 5D).

Finally, to confirm the specificity of the *miR-129-2-3p* mimic, the expression of *Casp6* and *Ccr2* was examined at the wound site in day 3 from application of mimic or mutant control immediately after wounding in db mice. The results showed that the expression of *Casp6* and *Ccr2* were significantly decreased in mimic-treated D3W [expression level (mean ± SD): *Casp6*: mutation: 1.1 ± 0.12, mimic: 0.85 ± 0.17,

p=0.016; *Ccr2*: mutation: 1.3 ± 0.25, mimic: 0.96 ± 0.22, *p*=0.029] (Fig. 5E-F).

Taken together, these results strongly suggest that the *miR-129-2-3p* mimic was effective at regulating gene expression in diabetic-derived neutrophils and could potentially rescue biological processes such as apoptosis in diabetic-derived neutrophils in the wound healing process. This would result in an improvement in delayed wound healing (Fig. 6), although this does not completely rule out the possibility that *miR-129-2-3p* may also impact the behavior of other cells *in vivo*, and that this may also contribute to enhanced healing.

DISCUSSION

Wound healing is a complex process that comprises inflammatory, proliferative, and remodeling phases. Bone marrow-derived cells (BMDCs) migrate to and participate in the homeostasis of skin tissue. After cutaneous injury, a heterogeneous population of BMDCs are recruited to the site of injury and contribute directly to the repair process by differentiating into various types of skin cells, such as fibroblasts, keratinocytes, and endothelial cells (21-22). They can also indirectly modulate repair and regeneration by producing cytokines and growth factors that promote re-epithelialization, neovascularization, and wound closure at the site of injury (23). In diabetic patients and animal models of diabetes, BMDCs, including neutrophils, contribute to an impaired healing/chronic wound environment by prolonging the inflammatory response and/or failing to promote the regenerative phase of wound healing (24-26). Neutrophils are the first immune cells recruited to the injured site in acute wound inflammation; they constitute up to 50% of the cells during the early phase of inflammation (5) and prevent microbe invasion through the process of phagocytosis (27). We previously showed that

the recruitment and/or retention kinetics of a heterogeneous population of BMDCs, including neutrophils, in diabetic cutaneous wounds are aberrant, leading to prolonged inflammation (5). These cells constitute the first subset of leukocytes to localize to injured tissue and may influence the entire localized inflammatory response.

miRNAs have been reported to be involved in both innate and adaptive immune responses (10); however, their role and regulation in neutrophils in the diabetic environment have remained unknown. To shed light on their possible role in dysfunction of diabetic-derived neutrophils, we examined miRNA expression and function in diabetic-derived neutrophils. Interestingly, the results showed that the expression of miRNAs involved in the inflammatory response changed in diabetic-derived neutrophils. Regarding *miR-223*, the expression of which was increased in diabetic-derived neutrophils in our study, it was reported to be associated with cell proliferation, apoptosis, migration, and invasion in gastric cancer (28). We further elucidated the function of *miR-223* in skin wound healing by analyzing *miR-223* knockout mice (29). Similarly, regarding *miR-31*, it was highly expressed during the transition from the inflammatory to the proliferative phase in vivo human skin wound healing model, and the overexpression of *miR-31* promoted cell proliferation and migration in human primary keratinocytes (30). Regarding *miR-149*, the expression of which was decreased, its target genes were shown to be involved in cell proliferation and apoptosis in patients suffering from acute injuries of the skin (31). These miRNAs might thus be involved in cell proliferation, migration, and apoptosis in diabetic-derived neutrophils. A recent paper shows that one of the factors associated with delayed wound healing in type 2 diabetic mice is Dnmt1-dependent dysregulation of hematopoietic stem cell (HSC) differentiation towards macrophages, and that the expression of Dnmt1

is regulated by miRNAs (32). In our study, the expression of miRNAs and mRNAs was significantly altered in diabetic-derived neutrophils, and this was associated with impaired wound healing. Alterations in gene expression in diabetic-derived neutrophils might be predetermined at the level of HSCs as described above, and epigenetic modifications in HSCs may be induced by type 2 diabetes mellitus.

In this study, microarray and qRT-PCR showed that the expression of *miR-129-2-3p* was downregulated in diabetic-derived neutrophils. Other recent studies have shown that *miR-129-2* is regulated epigenetically by DNA methylation (33). Analysis of ChIP data of the regulatory region in putative intron 1 of the gene (~4000 bp upstream of the sequence encoding the mature miRNA) showed that this region is bound by many transcription factors, including Pu.1 and Cebp transcription factors, both of which are underexpressed in diabetic-derived Gr-1^{+}CD11b^{+} myeloid cells (34), which include neutrophils (Supplementary Fig. 4A–B). Thus, it is possible that the decrease in these transcription factors in diabetic-derived neutrophils contributes to the decreased expression of *miR-129-2-3p*. There are also reports that *miR-129* family members are associated with proliferation and apoptosis in some types of cancer such as esophageal carcinoma and breast cancer (35-36). Moreover, Wang *et al.* reported that the topical administration of miR-129 agomir in diabetic animals promoted diabetic wound healing (37). GO and pathway analyses in this study also indicated that the predicted target genes of *miR-129-2-3p* are involved in a number of biological processes, including the inflammatory response, neutrophil chemotaxis, phagocytosis, and the execution phase of apoptosis, and are associated with multiple pathways such as cell differentiation, Toll-like receptor signaling, chemokine signaling, IL-6 signaling, and the inflammatory response pathway. We thus hypothesized that *miR-129-2-3p* in particular might be

involved in the functional regulation of diabetic-derived neutrophils in chronic inflammatory processes.

Neutrophils are constantly produced in large numbers in BM, and by definition the same numbers of cells must die or migrate away within a defined time period for homeostasis to be maintained (6). Several studies have also suggested that the caspase family plays an important role in both spontaneous and Fas receptor-mediated apoptosis in neutrophils (38-40). The activation of death receptors with Fas ligand is involved in the activation of *Casp8*, which is actually a component of the death-induced signaling complex (DISC) and activates downstream signaling. The activation of *Casp8* has been noted in neutrophils and the inactivation of this protease was shown to delay apoptosis (38). In this study, the expression of *Casp8* was significantly increased in db skin wound on D2W. In addition, the expression of *Casp6*, which is a downstream executioner caspase, also increased in db skin wound on D2W. These results suggest that apoptosis of neutrophils in db skin wound sites on D2W might be facilitated and/or inhibited by the activation of *Casp8* and/or the direct regulation of *Casp6* (41). *Ccr2* is a chemokine receptor expressed in monocytes and lymphocytes, but not in neutrophils. However, its expression changes under acute inflammation or in response to specific inflammatory stimuli in wounds. In mice with severe sepsis, *Ccr2* is expressed in neutrophils (42-46) and wound recruitment is controlled by *Ccr2* (47, 48). Accordingly, *Ccr2* expression on diabetic-derived neutrophils may be critical for chronic inflammation. In this study, the expression of *Ccr2* was also significantly increased in D2W. Thus, diabetic-derived neutrophils from BM may be excessively recruited to wound sites on D2W.

Previously, we showed that the numbers of myeloid cells, including neutrophils, in cutaneous wounds were significantly increased on day 2 after wounding, and the recruitment and/or accumulation kinetics of these cells were altered (5). In this study, the expression levels of *Casp6* and *Ccr2* in D2W of db increased compared with those in non-db. Moreover, our results showed that *miR-129-2-3p* directly regulated *Casp6* and *Ccr2* translation. Our *in vivo* analysis showed that skin wound healing in db was significantly accelerated from day 7. These results strongly suggest that the recruitment and accumulation kinetics of diabetic-derived neutrophils might be improved by overexpression of *miR-129-2-3p*, resulting in improved wound healing.

In conclusion, miRNAs are differentially expressed in diabetic-derived neutrophils compared with their levels in non-diabetic-derived neutrophils, particularly *miR-129-2-3p*. Our results suggest that *miR-129-2-3p* directly regulates *Casp6* and *Ccr2* translation, and is involved in inflammatory responses, apoptosis, chemotaxis, phagocytosis, and endocytosis. These findings further suggest that the deregulation of *miR-129-2-3p* contributes to the dysfunction of diabetic-derived neutrophils. The retention kinetics of neutrophils and chronic inflammation may be initiated via *miR-129-2-3p*-regulated genes such as *Casp6* and *Ccr2*. Accordingly, we suggest that *miR-129-2-3p* might be involved in the cellular kinetics and functional regulation of wound-recruited neutrophils and as such may prove to be a useful target for manipulation in a clinical context.

REFERENCES

1. Wicks K, Torbica T, Mace KA: Myeloid cell dysfunction and the pathogenesis of the diabetic chronic wound. Semin Immunol 2014;26:341-353
2. Singer AJ, Clark RA: Cutaneous wound healing. N Engl J Med 1999;341:738-746
3. Eming SA, Krieg T, Davidson JM: Inflammation in wound repair: molecular and cellular mechanisms. J Invest Dermatol 2007;127:514-525
4. Williams MD, Nadler JL: Inflammatory mechanisms of diabetic complications. Curr Diab Rep 2007;7:242-248
5. Mahdipour E, Charnock JC, Mace KA: Hoxa3 promotes the differentiation of hematopoietic progenitor cells into proangiogenic Gr-1+CD11b+ myeloid cells. Blood 2011;117:815-826
6. Simon HU: Neutrophil apoptosis pathways and their modifications in inflammation. Immunol Rev 2003;193:101-110
7. Bannon P, Wood S, Restivo T, Campbell L, Hardman MJ, Mace KA: Diabetes induces stable intrinsic changes to myeloid cells that contribute to chronic inflammation during wound healing in mice. Dis Model Mech 2013;6:1434-1447
8. Bartel DP: MicroRNAs: genomics, biogenesis, mechanism, and function. Cell 2004;116:281-297
9. Ambros V: The functions of animal microRNAs. Nature 2004;431:350-355
10. Recchiuti A, Krishnamoorthy S, Fredman G, Chiang N, Serhan CN: MicroRNAs in resolution of acute inflammation: identification of novel resolvin D1-miRNA circuits. FASEB J 2011;25:544-560
11. Baek D, Villén J, Shin C, Camargo FD, Gygi SP, Bartel DP: The impact of microRNAs on protein output. Nature 2008;455:64-71

12. Selbach M, Schwanhäusser B, Thierfelder N, Fang Z, Khanin R, Rajewsky N: Widespread changes in protein synthesis induced by microRNAs. Nature 2008;455:58-63

13. Suresh Babu S, Thandavarayan RA, Joladarashi D, Jeyabal P, Krishnamurthy S, Bhimaraj A, Youker KA, Krishnamurthy P: MicroRNA-126 overexpression rescues diabetes-induced impairment in efferocytosis of apoptotic cardiomyocytes. Sci Rep 2016;6:36207

14. Wu Y, Zhong JL, Hou N, Sun Y, Ma B, Nisar MF, Teng Y, Tan Z, Chen K, Wang Y, Yang X: MicroRNA Let-7b inhibits keratinocyte migration in cutaneous wound healing by targeting IGF2BP2. Exp Dermatol 2017;26:116-123

15. Li X, Li D, Wang A, Chu T, Lohcharoenkal W, Zheng X, Grünler J, Narayanan S, Eliasson S, Herter EK, Wang Y, Ma Y, Ehrström M, Eidsmo L, Kasper M, Pivarcsi A, Sonkoly E, Catrina SB, Ståhle M, Xu Landén N: MicroRNA-132 with Therapeutic Potential in Chronic Wounds. J Invest Dermatol 2017;137:2630-2638

16. Wang JM, Tao J, Chen DD, Cai JJ, Irani K, Wang Q, Yuan H, Chen AF: MicroRNA miR-27b rescues bone marrow-derived angiogenic cell function and accelerates wound healing in type 2 diabetes mellitus. Arterioscler Thromb Vasc Biol 2014;34:99-109

17. Dangwal S, Stratmann B, Bang C, Lorenzen JM, Kumarswamy R, Fiedler J, Falk CS, Scholz CJ, Thum T, Tschoepe D: Impairment of Wound Healing in Patients With Type 2 Diabetes Mellitus Influences Circulating MicroRNA Patterns via Inflammatory Cytokines. Arterioscler Thromb Vasc Biol 2015;35:1480-1488

18. Tanaka K, Kim SE, Yano H, Matsumoto G, Ohuchida R, Ishikura Y, Araki M, Araki K, Park S, Komatsu T, Hayashi H, Ikematsu K, Hirano A, Martin P,

Shimokawa I, Mori R: MiR-142 Is Required for Staphylococcus aureus Clearance at Skin Wound Sites via Small GTPase-Mediated Regulation of the Neutrophil Actin Cytoskeleton. J Invest Dermatol 2017;137:931-940

19. Schmittgen TD, Livak KJ: Analyzing real-time PCR data by the comparative C(T) method. Nat Protoc 2008;3:1101-1108
20. Mori R, Tanaka K, de Kerckhove M, Okamoto M, Kashiyama K, Kim S, Kawata T, Komatsu T, Park S, Ikematsu K, Hirano A, Martin P, Shimokawa I: Reduced FOXO1 expression accelerates skin wound healing and attenuates scarring. Am J Pathol 2014;184:2465-2479
21. Badiavas EV, Abedi M, Butmarc J, Falanga V, Quesenberry P: Participation of bone marrow derived cells in cutaneous wound healing. J Cell Physiol 2003;196:245-250
22. Brittan M, Braun KM, Reynolds LE, Conti FJ, Reynolds AR, Poulsom R, Alison MR, Wright NA, Hodivala-Dilke KM: Bone marrow cells engraft within the epidermis and proliferate in vivo with no evidence of cell fusion. J Pathol 2005;205:1-13
23. Eming SA, Krieg T, Davidson JM: Inflammation in wound repair: molecular and cellular mechanisms. J Invest Dermatol 2007;127:514-525
24. Tepper OM, Galiano RD, Capla JM, Kalka C, Gagne PJ, Jacobowitz GR, Levine JP, Gurtner GC: Human endothelial progenitor cells from type II diabetics exhibit impaired proliferation, adhesion, and incorporation into vascular structures. Circulation 2002;106:2781-2786

25. Awad O, Jiao C, Ma N, Dunnwald M, Schatteman GC: Obese diabetic mouse environment differentially affects primitive and monocytic endothelial cell progenitors. Stem Cells 2005;23:575-583

26. Mace KA, Restivo TE, Rinn JL, Paquet AC, Chang HY, Young DM, Boudreau NJ: HOXA3 modulates injury-induced mobilization and recruitment of bone marrow-derived cells. Stem Cells 2009;27:1654-1665

27. Su Y, Richmond A: Chemokine Regulation of Neutrophil Infiltration of Skin Wounds. Adv Wound Care (New Rochelle) 2015;4:631-640

28. Li J, Guo Y, Liang X, Sun M, Wang G, De W, Wu W: MicroRNA-223 functions as an oncogene in human gastric cancer by targeting FBXW7/hCdc4. J Cancer Res Clin Oncol 2012;138:763-774

29. de Kerckhove M, Tanaka K, Umehara T, Okamoto M, Kanematsu S, Hayashi H, Yano H, Nishiura S, Tooyama S, Matsubayashi Y, Komatsu T, Park S, Okada Y, Takahashi R, Kawano Y, Hanawa T, Iwasaki K, Nozaki T, Torigoe H, Ikematsu K, Suzuki Y, Tanaka K, Martin P, Shimokawa I, Mori R: Targeting *miR-223* in neutrophils enhances the clearance of *Staphylococcus aureus* in infected wounds. EMBO Mol Med 2018; e9024.

30. Li D, Li XI, Wang A, Meisgen F, Pivarcsi A, Sonkoly E, Ståhle M, Landén NX: MicroRNA-31 Promotes Skin Wound Healing by Enhancing Keratinocyte Proliferation and Migration. J Invest Dermatol 2015;135:1676-1685

31. Li P, He Q, Luo C, Qian L: Differentially expressed miRNAs in acute wound healing of the skin: a pilot study. Medicine (Baltimore) 2015;94:e458

32. Yan J, Tie G, Wang S, Tutto A, DeMarco N, Khair L, Fazzio TG, Messina LM: Diabetes impairs wound healing by Dnmt1-dependent dysregulation of

hematopoietic stem cells differentiation towards macrophages. Nat Commun 2018;9:33

33. Xiao Y, Li X, Wang H, Wen R, He J, Tang J: Epigenetic regulation of miR-129-2 and its effects on the proliferation and invasion in lung cancer cells. J Cell Mol Med 2015;19:2172-2180
34. Wicks K, Torbica T, Umehara T, Amin S, Bobola N, Mace KA: Diabetes Inhibits Gr-1+ Myeloid Cell Maturation via Cebpa Deregulation. Diabetes 2015;64:4184-4197
35. Kang M, Li Y, Liu W, Wang R, Tang A, Hao H, Liu Z, Ou H: miR-129-2 suppresses proliferation and migration of esophageal carcinoma cells through downregulation of SOX4 expression. Int J Mol Med 2013;32:51-58
36. Tang X, Tang J, Liu X, Zeng L, Cheng C, Luo Y, Li L, Qin SL, Sang Y, Deng LM, Lv XB: Downregulation of miR-129-2 by promoter hypermethylation regulates breast cancer cell proliferation and apoptosis. Oncol Rep 2016;35:2963-2969
37. Wang W, Yang C, Wang XY, Zhou LY, Lao GJ, Liu D, Wang C, Hu MD, Zeng TT, Yan L, Ren M: MicroRNA-129 and -335 Promote Diabetic Wound Healing by Inhibiting Sp1-Mediated MMP-9 Expression. Diabetes 2018.
38. Daigle I, Simon HU: Critical role for caspases 3 and 8 in neutrophil but not eosinophil apoptosis. Int Arch Allergy Immunol 2001;126:147-156
39. Pongracz J, Webb P, Wang K, Deacon E, Lunn OJ, Lord JM: Spontaneous neutrophil apoptosis involves caspase 3-mediated activation of protein kinase C-delta. J Biol Chem 1999;274:37329-37334
40. Khwaja A, Tatton L: Caspase-mediated proteolysis and activation of protein kinase Cdelta plays a central role in neutrophil apoptosis. Blood 1999;94:291-301

41. Zhao R, Guan DW, Zhang W, Du Y, Xiong CY, Zhu BL, Zhang JJ: Increased expressions and activations of apoptosis-related factors in cell signaling during incised skin wound healing in mice: a preliminary study for forensic wound age estimation. Leg Med (Tokyo) 2009;11 Suppl 1:S155-160

42. Maus UA, Waelsch K, Kuziel WA, Delbeck T, Mack M, Blackwell TS, Christman JW, Schlöndorff D, Seeger W, Lohmeyer J: Monocytes are potent facilitators of alveolar neutrophil emigration during lung inflammation: role of the CCL2-CCR2 axis. J Immunol 2003;170:3273-3278

43. Dewald O, Zymek P, Winkelmann K, Koerting A, Ren G, Abou-Khamis T, Michael LH, Rollins BJ, Entman ML, Frangogiannis NG: CCL2/Monocyte Chemoattractant Protein-1 regulates inflammatory responses critical to healing myocardial infarcts. Circ Res 2005;96:881-889

44. Rios-Santos F, Alves-Filho JC, Souto FO, Spiller F, Freitas A, Lotufo CM, Soares MB, Dos Santos RR, Teixeira MM, Cunha FQ: Down-regulation of CXCR2 on neutrophils in severe sepsis is mediated by inducible nitric oxide synthase-derived nitric oxide. Am J Respir Crit Care Med 2007;175:490-497

45. Souto FO, Alves-Filho JC, Turato WM, Auxiliadora-Martins M, Basile-Filho A, Cunha FQ: Essential role of CCR2 in neutrophil tissue infiltration and multiple organ dysfunction in sepsis. Am J Respir Crit Care Med 2011;183:234-242

46. Speyer CL, Gao H, Rancilio NJ, Neff TA, Huffnagle GB, Sarma JV, Ward PA: Novel chemokine responsiveness and mobilization of neutrophils during sepsis. Am J Pathol 2004;165:2187-2196

47. Willenborg S, Lucas T, van Loo G, Knipper JA, Krieg T, Haase I, Brachvogel B, Hammerschmidt M, Nagy A, Ferrara N, Pasparakis M, Eming SA: CCR2 recruits

an inflammatory macrophage subpopulation critical for angiogenesis in tissue repair. Blood 2012;120:613-625

48. Devalaraja RM, Nanney LB, Du J, Qian Q, Yu Y, Devalaraja MN, Richmond A: Delayed wound healing in CXCR2 knockout mice. J Invest Dermatol 2000;115:234-244

ACKNOWLEDGMENTS

This work was supported in part by the Japan Society for the Promotion of Science (Grant-in-Aid for Young Scientists B, 15K20314 and 17K17021) and the Cell Science Research Foundation (Osaka, Japan). We thank Edanz Group (www.edanzediting.com/ac) for editing a draft of this manuscript.

Author contributions are as follows: T.U., R.M., K.A.M. and K.I. conceived the experiments; T.U., T.Y., T.M., and Y.A. conducted the experiments; and T.U. and R.M. analyzed the results. All authors reviewed the manuscript. T.U. is the guarantor of this work and, as such, had full access to all the data in the study and takes responsibility for the integrity of the data and the accuracy of the data analysis.

CONFLICT OF INTEREST

The authors declare that they have no conflicts of interest.

Table 1 List of Antibodies

Primary antibody (Manufacturer)	Species	Dilution	Blocking (Manufacturer)	Secondary antibody (Manufacturer)	Dilution
CASP6 (Cell Signaling Technology: 9762)	Rabbit	1:1000 (WB)	PVDF Blocking Reagent (TOYOBO)	Anti-Rabbit IgG HRP-linked whole antibody (GE Healthcare)	1:25,000
GAPDH (Abcam: ab9485)	Rabbit	1:1000 (WB)	PVDF Blocking Reagent (TOYOBO)	Anti-Rabbit IgG HRP-linked whole antibody (GE Healthcare)	1:25,000

WB: Western immunoblotting

Table 2 MicroRNAs expressing with moderated t-test (cut-off<0.05) and Storey with bootstrapping in diabetic-derived neutrophils compared with non-diabetic-derived neutrophils

Gene symbol	Fold difference (Db/Non-db)	Regulation	*p* value
mmu-miR-129-1-3p	-19.658678	down	0.00000004
mmu-miR-129-2-3p	-3.2003143	down	0.00022570
mmu-miR-129-5p	-91.52625	down	0.00010058
mmu-miR-20b-3p	-9.698807	down	0.00000449
mmu-miR-466c-5p	-23.062893	down	0.00000005
mmu-miR-669a-5p	-22.38164	down	0.00000007
mmu-miR-678	-15.44842	down	0.00127955
mmu-miR-6916-5p	-38.222507	down	0.00000010
mmu-miR-6997-5p	-29.356022	down	0.00000081
mmu-miR-770-3p	-15.649054	down	0.00122081

Table 3 GO analysis for genes predicted to be targets of miR129-2-3p

Gene symbol	Gene name
Inflammatory response	
Hyal3	Hyaluronoglucosaminidase 3
Casp6	Caspase 6
Ccr1l1	Chemokine (C-C motif) receptor 1-like 1
Ccr2	Chemokine (C-C motif) receptor 2
Havcr2	Hepatitis A virus cellular receptor 2
Myd88	Myeloid differentiation primary response gene 88
Cxcl5	Chemokine (C-X-C motif) ligand 5
Il23r	Interleukin 23 receptor
Tlr5	Toll-like receptor 5
Ccl24	Chemokine (C-C motif) ligand 24
Pycard	PYD and CARD domain containing
Vimp	VCP-interacting membrane protein
Lgals9	Lectin, galactose binding, soluble 9
Ppara	Peroxisome proliferator activated receptor alpha
Metrnl	Meteorin, glial cell differentiation regulator-like
Stat5a	Signal transducer and activator of transcription 5A
Execution phase of apoptosis	
Casp8	Caspase 8
Taok1	TAO kinase 1

Dedd2	Death effector domain-containing DNA binding protein 2
	Neutrophil chemotaxis
Ccl24	Chemokine (C-C motif) ligand 24
Vav3	Vav 3 oncogene
	Endocytosis
Ildr1	Immunoglobulin-like domain containing receptor 1
Arrb1	Arrestin, beta 1
Ache	Acetylcholinesterase
Grn	Granulin
Timd2	T cell immunoglobulin and mucin domain containing 2
Tmprss13	Transmembrane protease, serine 13
Micall1	Microtubule associated monooxygenase, calponin and LIM domain containing-like 1
Cltb	Clathrin, light polypeptide (Lcb)
Add1	Adducin 1 (alpha)
Cdh13	Cadherin 13
Cnn2	Calponin 2
Pycard	PYD and CARD domain containing
	Phagocytosis
Ccr2	Chemokine (C-C motif) receptor 2
Lepr	Leptin receptor
Treml4	Triggering receptor expressed on myeloid cells-like 4
Megf10	Multiple EGF-like-domains 10

FIGURE LEGENDS

Figure 1 A. Microarray analysis. A total of 10 miRNAs showed a level in diabetic-derived neutrophils that was less than half that in non-diabetic-derived neutrophils. B. Signal value with 90th percentile shift normalization of microarray for each miRNA. The data were log10-transformed. *mmu-let-7i-5p* and *mmu-miR-484* are control miRNAs. Graphs show mean ± SD, for which no statistical analysis was performed. C. Relative expression of *miR-129-2-3p* in neutrophils isolated from BM. *miR-129-2-3p* was downregulated in diabetic-derived neutrophils, as determined by qRT-PCR. D. Relative expression of *miR-129-2-3p* in neutrophils, macrophages, B cells, and T cells isolated from BM. *miR-129-2-3p* mainly expressed in neutrophils. Graphs show mean ± SD (n=5). The statistical significance of differences between means in Fig. 1C was assessed by Mann–Whitney *U* test. The statistical significance of differences between means in Fig. 1D was assessed by one-way ANOVA, followed by Tukey's multiple comparison test. $^{**}P < 0.01$; $^{***}P < 0.001$.

Figure 2 A-E. Relative expression of *Casp6*, *Ccr1l1*, *Ccr2*, *Casp8*, and *Dedd2* in neutrophils isolated from BM. *Casp6*, *Ccr1l1*, *Ccr2*, *Casp8*, and *Dedd2* were expressed at high levels in Db. Graphs show mean ± SD (n=5–7). The statistical significance of differences between means was assessed by Mann–Whitney *U* test. $^{**}P < 0.01$.

Figure 3 A. Alignment of *miR-129-2-3p* seed sequences and the corresponding seed sequences of *Casp6*, *Ccr2*, and *Dedd2* mRNA. *miR-129-2-3p* is predicted to bind with high affinity to *Casp6*, *Ccr2*, and *Dedd2* 3′-UTRs. B–D. A luciferase reporter vector encoding the 3′-UTRs was cotransfected with *miR-129-2-3p* mimic or mutation into

3T3 cells. A decrease in luciferase activity indicates binding of the miRNA mimic to the 3′-UTR of the target sequence. E–F. Relative expression of *CASP6* and *DEDD2* in HL-60 cells transfected with mutation or mimic. Graphs show mean ± SD (n=4-6). The statistical significance of differences between means was assessed by Mann–Whitney *U* test. **P* < 0.05; ***P* < 0.01.

Figure 4 A. Representative images of neutrophil IHC in skin wounds at D2W. Arrowhead indicates wound margin. *Scale bar* = 400 μm (upper) and 50 μm (lower). B. Ratios of neutrophil-positive area relative to the wound area at D1W and D2W in each skin wound (3-4 wounds), and the average value of each positive area was used for comparative analysis. C. ISH of *miR-129-2-3p* showing that wound-infiltrated neutrophils were predominantly present in the wound sites of non-db at D1W. *Scale bar* = 300 μm (upper) and 100 μm (lower). Arrowhead, wound margin. D. Relative expression of *miR-129-2-3p* in equal numbers of neutrophils from non-db and db D2W (each n=5). E–G. Relative expression of *Casp6*, *Ccr2*, and *Dedd2* in skin wounds on D2W. Graphs show mean ± SD (n=5–11). H. Relative expression of cleaved CASP6 to total CASP6 in skin wounds on D2W. Graphs show mean ± SD (4 wounds). The statistical significance of differences between means was assessed by Mann–Whitney *U* test. **P* < 0.05; ***P* < 0.01.

Figure 5 A. Representative images of the gross appearance of db excisional wounds with *miR-129-2-3p* mimic, mutation as a negative control and mutation in non-db. B. Proportion of wound area on each day after wounding (3, 7, 10, 14, and 21 days) relative to the initial wound area. Wound area was measured using Adobe Photoshop

CC. Graphs show mean ± SD (mutation in non-db: n=4, mutation and mimic in db: n=9). The statistical significance of differences between means was assessed by two-way ANOVA, followed by Bonferroni post-tests to compare replicate means. C. Representative images of neutrophil IHC in skin wounds at D3W with *miR-129-2-3p* mimic or mutation. Arrowhead, wound margin. *Scale bar* = 400 μm. D. Ratios of neutrophil-positive area relative to the wound area at D3W with mimic or mutation in each skin wound (3-4 wounds), and the average values of each positive area were used for comparative analysis. E–F. Relative expression of *Casp6* and *Ccr2* in skin wounds at D3W with *miR-129-2-3p* mimic or mutation. Graphs show mean ± SD (4-8 wounds). The statistical significance of differences between means was assessed by Mann–Whitney *U* test. **P* < 0.05; ***P* < 0.01; ****P* < 0.001.

Figure 6 Model summarizing the interplay among *miR-129-2-3p*, *Casp6*, and *Ccr2* in diabetic-derived neutrophils from bone marrow to wound site.

Figure. 1

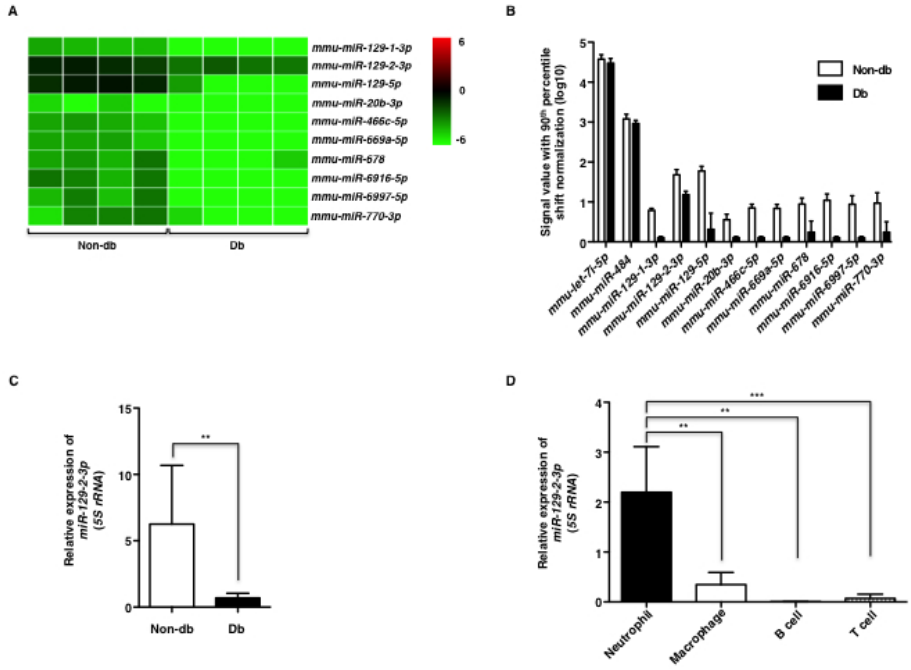

Figure 1 A. Microarray analysis. A total of 10 miRNAs showed a level in diabetic-derived neutrophils that was less than half that in non-diabetic-derived neutrophils. B. Signal value with 90th percentile shift normalization of microarray for each miRNA. The data were log10-transformed. mmu-let-7i-5p and mmu-miR-484 are control miRNAs. Graphs show mean ± SD, for which no statistical analysis was performed. C. Relative expression of miR-129-2-3p in neutrophils isolated from BM. miR-129-2-3p was downregulated in diabetic-derived neutrophils, as determined by qRT-PCR. D. Relative expression of miR-129-2-3p in neutrophils, macrophages, B cells, and T cells isolated from BM. miR-129-2-3p mainly expressed in neutrophils. Graphs show mean ± SD (n=5). The statistical significance of differences between means in Fig. 1C was assessed by Mann–Whitney U test. The statistical significance of differences between means in Fig. 1D was assessed by one-way ANOVA, followed by Tukey's multiple comparison test. **P < 0.01; ***P < 0.001.

254x190mm (72 x 72 DPI)

Figure. 2

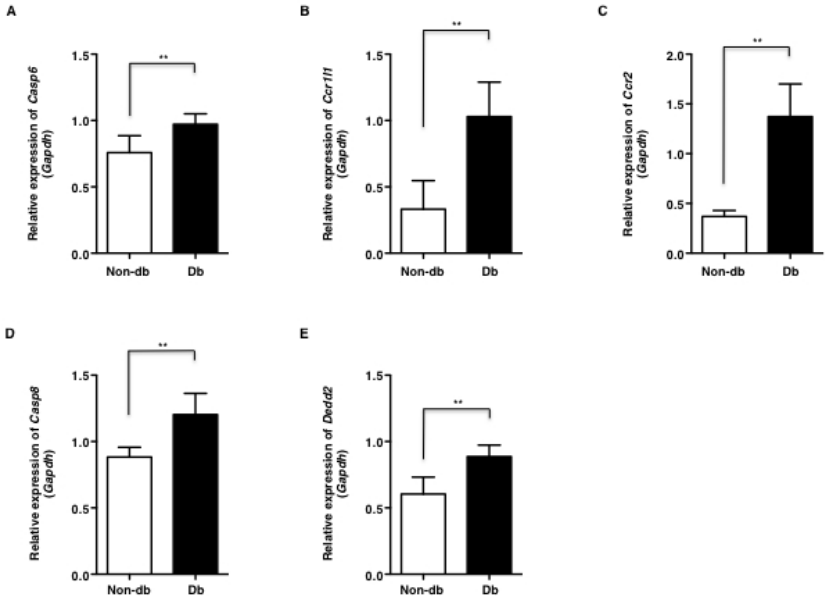

Figure 2 A-E. Relative expression of Casp6, Ccr1l1, Ccr2, Casp8, and Dedd2 in neutrophils isolated from BM. Casp6, Ccr1l1, Ccr2, Casp8, and Dedd2 were expressed at high levels in Db. Graphs show mean ± SD (n=5–7). The statistical significance of differences between means was assessed by Mann–Whitney U test. **P < 0.01.

254x190mm (72 x 72 DPI)

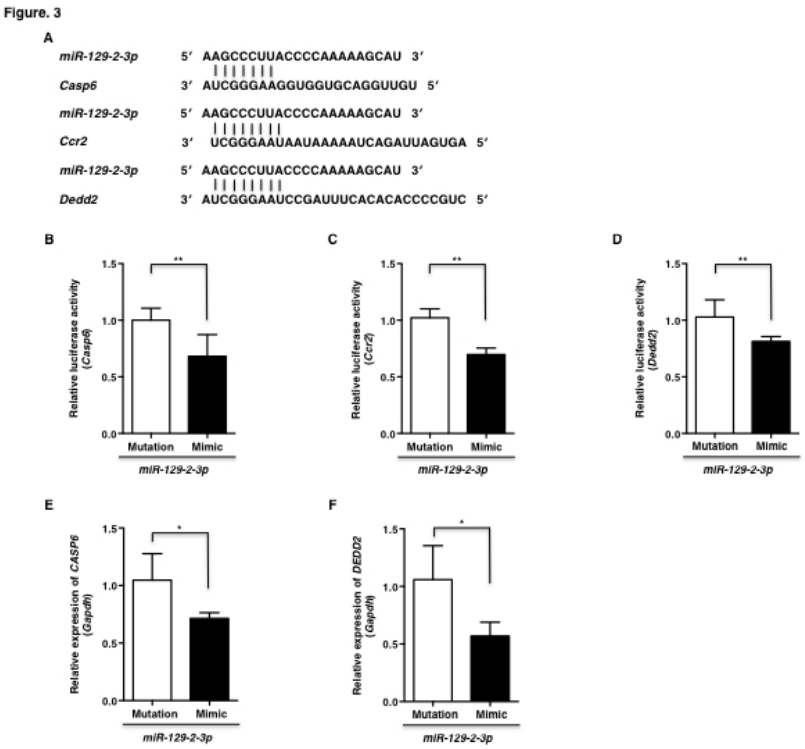

Figure 3 A. Alignment of miR-129-2-3p seed sequences and the corresponding seed sequences of Casp6, Ccr2, and Dedd2 mRNA. miR-129-2-3p is predicted to bind with high affinity to Casp6, Ccr2, and Dedd2 3′-UTRs. B–D. A luciferase reporter vector encoding the 3′-UTRs was cotransfected with miR-129-2-3p mimic or mutation into 3T3 cells. A decrease in luciferase activity indicates binding of the miRNA mimic to the 3′-UTR of the target sequence. E–F. Relative expression of CASP6 and DEDD2 in HL-60 cells transfected with mutation or mimic. Graphs show mean ± SD (n=4-6). The statistical significance of differences between means was assessed by Mann–Whitney U test. *P < 0.05; **P < 0.01.

254x190mm (72 x 72 DPI)

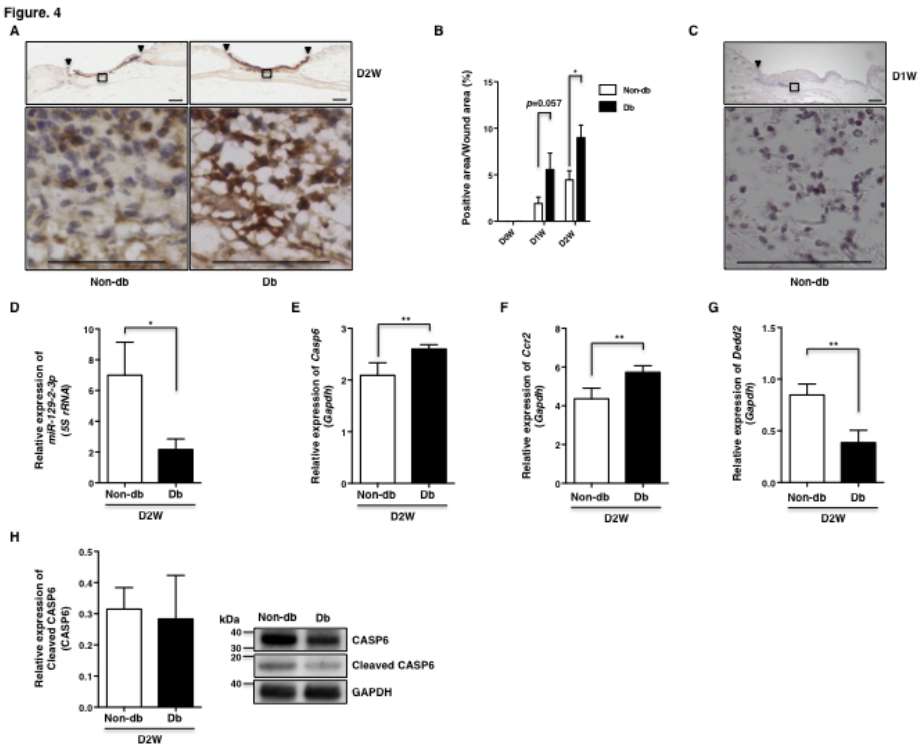

Figure 4 A. Representative images of neutrophil IHC in skin wounds at D2W. Arrowhead indicates wound margin. Scale bar = 400 μm (upper) and 50 μm (lower). B. Ratios of neutrophil-positive area relative to the wound area at D1W and D2W in each skin wound (3-4 wounds), and the average value of each positive area was used for comparative analysis. C. ISH of miR-129-2-3p showing that wound-infiltrated neutrophils were predominantly present in the wound sites of non-db at D1W. Scale bar = 300 μm (upper) and 100 μm (lower). Arrowhead, wound margin. D. Relative expression of miR-129-2-3p in equal numbers of neutrophils from non-db and db D2W (each n=5). E–G. Relative expression of Casp6, Ccr2, and Dedd2 in skin wounds on D2W. Graphs show mean ± SD (n=5–11). H. Relative expression of cleaved CASP6 to total CASP6 in skin wounds on D2W. Graphs show mean ± SD (4 wounds). The statistical significance of differences between means was assessed by Mann–Whitney U test. *P < 0.05; **P < 0.01.

254x190mm (72 x 72 DPI)

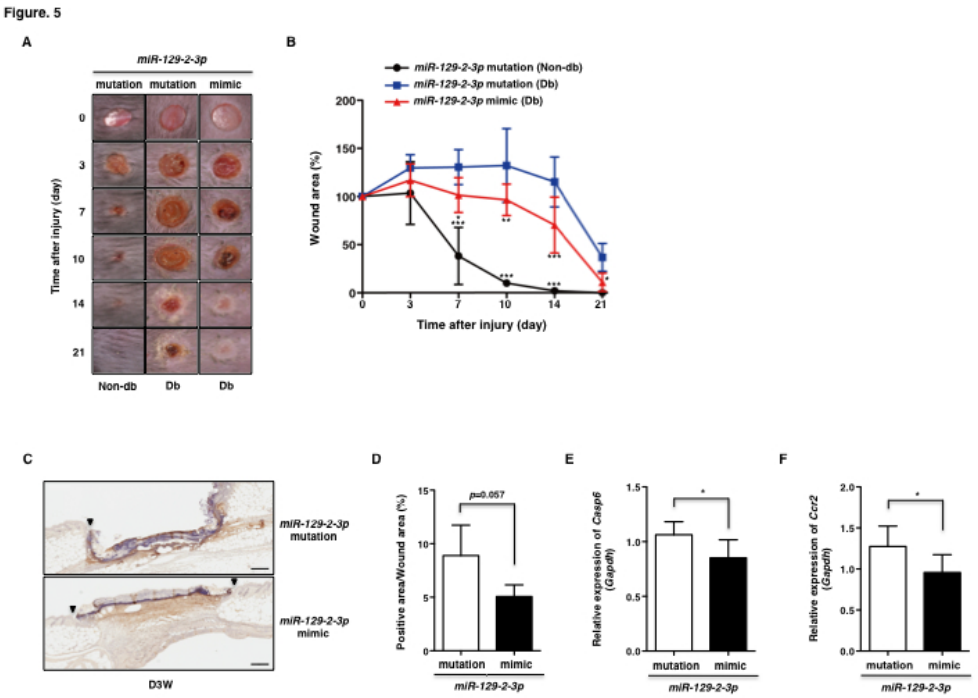

Figure 5 A. Representative images of the gross appearance of db excisional wounds with miR-129-2-3p mimic, mutation as a negative control and mutation in non-db. B. Proportion of wound area on each day after wounding (3, 7, 10, 14, and 21 days) relative to the initial wound area. Wound area was measured using Adobe Photoshop CC. Graphs show mean ± SD (mutation in non-db: n=4, mutation and mimic in db: n=9). The statistical significance of differences between means was assessed by two-way ANOVA, followed by Bonferroni post-tests to compare replicate means. C. Representative images of neutrophil IHC in skin wounds at D3W with miR-129-2-3p mimic or mutation. Arrowhead, wound margin. Scale bar = 400 μm. D. Ratios of neutrophil-positive area relative to the wound area at D3W with mimic or mutation in each skin wound (3-4 wounds), and the average values of each positive area were used for comparative analysis. E–F. Relative expression of Casp6 and Ccr2 in skin wounds at D3W with miR-129-2-3p mimic or mutation. Graphs show mean ± SD (4-8 wounds). The statistical significance of differences between means was assessed by Mann–Whitney U test. *P < 0.05; **P < 0.01; ***P < 0.001.

254x190mm (72 x 72 DPI)

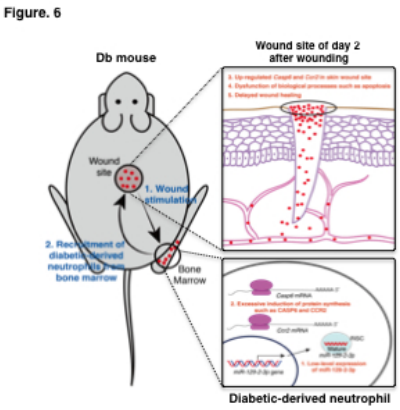

Figure 6 Model summarizing the interplay among miR-129-2-3p, Casp6, and Ccr2 in diabetic-derived neutrophils from bone marrow to wound site.

254x190mm (72 x 72 DPI)

SUPPLEMENTARY FIGURE LEGENDS

Figure 1 Microarray fold change analysis. A. The expression level of 22 miRNAs in diabetic-derived neutrophils was more than double that in non-diabetic-derived neutrophils. B. The expression level of 80 miRNAs was decreased to less than half in fold change analysis.

Figure 2 Relative expression of *miR-129-2-3p* in neutrophils, macrophages, B cells and T cells isolated from mouse spleen. Graphs show mean ± SD (n=2-3). The statistical analysis was not performed.

Figure 3 Candidate target genes of miRNAs in Table 2. More than 800 mRNAs were predicted to be targets of the miRNAs using GeneSpring.

Figure 4 A. Relative expression of *Casp8* in skin wound on day 2 after wounding. Graph shows mean ± SD (n=6–11). $^{**}P < 0.01$. B. Double-label fIHC for neutrophils (α-Ly-6G) and CASP6 or CCR2 shows neutrophils and CASP6 or CCR2 in D2W of db. Nuclei were counterstained with DAPI and CASP6- or CCR2-expressing neutrophils (arrowheads). Scale bar = 10 μm.

Figure 5 A-B. The mechanism of the deregulation of *miR-129-2-3p* expression in the diabetic derived neutrophils. Analysis of ChIP data of the regulatory region in the putative intron 1 of the gene (~4000bp upstream of the sequence encoding the mature miR) showed that this region is bound by many transcription factors, including Pu.1 and Cebp transcription factors, both of which are underexpressed in diabetic-derived

Gr-1+CD11b+ myeloid cells, which include neutrophils. Thus it is possible that the decrease in these transcription factors in diabetic-derived neutrophils contributes to the decreased expression of *miR-129-2-3p*.

Supplementary Fig. 1

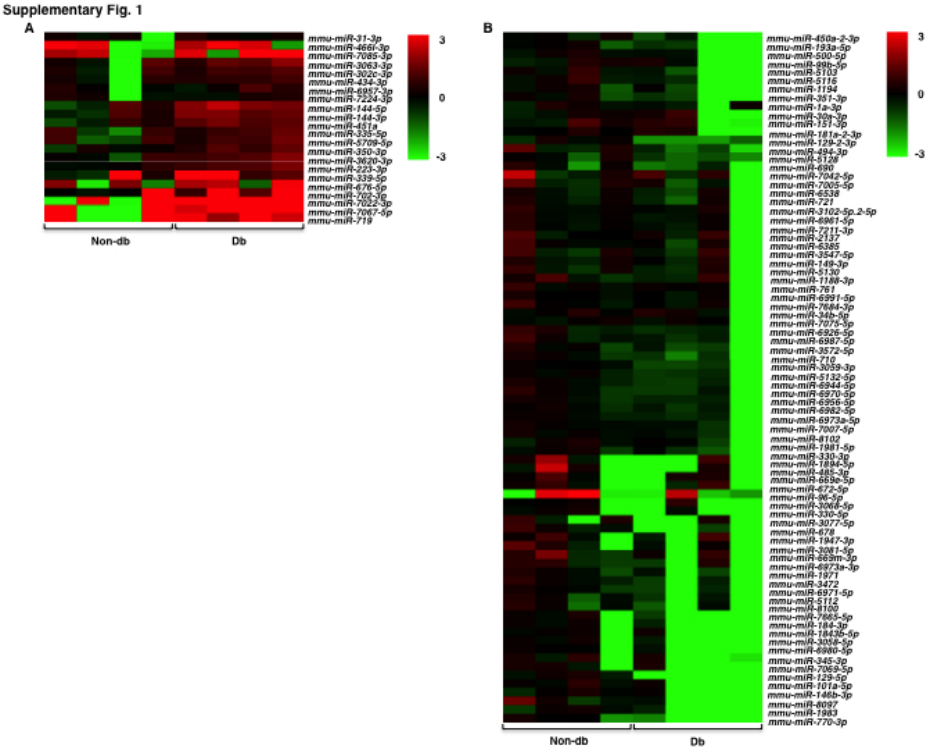

254x190mm (72 x 72 DPI)

Supplementary Fig. 2

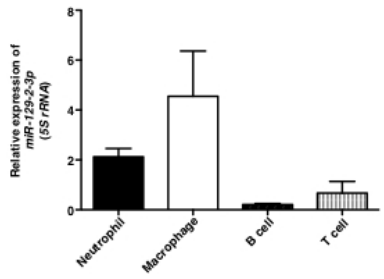

254x190mm (72 x 72 DPI)

Supplementary Fig. 3

Gene symbol	p-value
3-Mar	0.01461033
0610040J01Rik	0.04183969
1700017B05Rik	0.03919376
1700020L24Rik	0.02318626
1700025G04Rik	0.01388870
1700030M09Rik	0.00209661
1700102H20Rik	0.04585586
1810010H24Rik	0.00282878
2210010C04Rik	0.03312228
4930528D03Rik	0.02477176
4930563D23Rik	0.01498096
4930563I02Rik	0.03802471
4930578C19Rik	0.04585586
4933407E24Rik	0.02883412
5031434O11Rik	0.01063142
5430419D17Rik	0.01261794
5430427M07Rik	0.03441095
9030624J02Rik	0.02352948
A230009B12Rik	0.00198833
A230056P14Rik	0.00916503
A230103J11Rik	0.02675881
A530072M11Rik	0.03739224
A630001G21Rik	0.03927401
Aaed1	0.03919581
Aard	0.00027853
Abca2	0.00425318
Abcd4	0.04372614
Abce1	0.04695308
Ablim3	0.00734268
Abracl	0.02575428
Abtb1	0.02877674
Acaca	0.02641597
Acad8	0.02555540
Acbd4	0.04449480
Acbd6	0.00853320
Ache	0.04606521
Acot1	0.03075305
Acp1	0.00756649
Acp5	0.04372614
Acpp	0.04340294
Actl9	0.00127532
Adam7	0.02352948

Adamts13	0.02499234
Add1	0.00469941
Adgre5	0.01690706
Adgrf3	0.00456050
Adgrl4	0.00876244
Adh6a	0.01505858
Adssl1	0.04606521
Agpat5	0.01424618
Agtrap	0.01498096
Akap2	0.03830510
Aldh3a1	0.01975150
Aldh3b3	0.03927401
Aldh4a1	0.03802471
Amer1	0.02499043
Amica1	0.01016593
Amy2b	0.02959118
Angpt2	0.01025080
Angptl4	0.00802722
Ankdd1b	0.00046165
Ano5	0.02898848
Ap1ar	0.00610165
Ap3s2	0.01402938
Apln	0.04104947
Arhgap32	0.04585586
Arhgef40	0.00205223
Arl16	0.04054567
Arpc1b	0.00905818
Arpc4	0.00381840
Arrb1	0.00951772
Arsg	0.02883412
Atg10	0.02696755
Atg4b	0.01311951
Atp2b4	0.04315608
Atp6v0d2	0.03071801
Atp7a	0.03564442
AU041133	0.02994245
AV320801	0.00853320
Avil	0.00960236
Avpi1	0.01016593
AW121686	0.00425318
B2m	0.03325104
B3galt1	0.01296667
B3gnt3	0.02778541
B4galnt2	0.00090347

B9d2	0.00255464
Baalc	0.03479049
Bank1	0.00341667
Bard1	0.01183101
BC026585	0.01656024
BC051019	0.04372614
BC089491	0.02685617
Bcas3	0.04295983
Bean1	0.00028429
Bet1l	0.04449480
Bglap	0.00335240
Bmp6	0.01197494
Bpifa2	0.04845232
Bsnd	0.01922092
Btbd10	0.03071801
Bysl	0.02842969
Bzw2	0.02917970
C1ql2	0.01197494
C1rl	0.01449990
C430049E01Rik	0.03679777
Cacna1d	0.00138424
Caln1	0.03211343
Calu	0.04447339
Casp6	0.03559319
Casp8	0.00134419
Cat	0.00560699
Catsper4	0.04845232
Catsperg1	0.01009301
Cbwd1	0.02575428
Ccbl2	0.02287248
Ccdc141	0.04183969
Ccdc160	0.03679777
Ccdc167	0.02289127
Ccdc182	0.01362100
Ccdc43	0.03312228
Ccdc64b	0.04372614
Ccdc67	0.02842969
Ccdc77	0.04864488
Cckbr	0.00723546
Ccl1	0.04372614
Ccl24	0.01197494
Ccp110	0.04287131
Ccr10	0.00499851
Ccr1l1	0.01656024

Ccr2	0.04130955
Cd19	0.04864488
Cd200r2	0.04449480
Cd300ld	0.03651165
Cd38	0.04492528
Cd3eap	0.00335240
Cdh13	0.00341667
Cdhr1	0.04902307
Cdip1	0.00536626
Cdk14	0.03959969
Celf5	0.02099694
Cenpb	0.03927401
Cep131	0.00743287
Cep162	0.01063142
Cep350	0.01574350
Cfap77	0.00577459
Chst10	0.04054365
Chst5	0.03441095
Cir1	0.02990500
CK137956	0.00544523
Clasp1	0.04780030
Clec4a4	0.00743287
Clptm1	0.02842969
Clrn3	0.04492528
Cltb	0.04295983
Clvs1	0.03682372
Cmtm7	0.02994245
Cnih4	0.01980136
Cnn2	0.00013783
Cnp	0.00694384
Col3a1	0.03545622
Col5a1	0.00140651
Commd4	0.01812491
Coq3	0.04393565
Cox10	0.04723923
Cpm	0.00000442
Cpne1	0.04902307
Crispld2	0.02917970
Cryab	0.00068275
Csrp2	0.04143602
Cstf1	0.03075305
Ctsr	0.00335240
Ctu1	0.04864488
Cxcl5	0.01865191

Cxxc5	0.01613505
Cyb5r3	0.03564442
Cyp2e1	0.04143602
D230017M19Rik	0.00666047
D630003M21Rik	0.03559319
Dbx2	0.02625527
Dcaf10	0.01277185
Dcbld1	0.01156704
Dclre1b	0.02409291
Ddr2	0.00067410
Ddx55	0.00467559
Dedd2	0.01135205
Dennd6b	0.00424170
Dgki	0.02044872
Dhrs4	0.01769506
Dhrs7b	0.04372614
Dlgap2	0.01449990
Dlgap4	0.00040622
Dlk1	0.00057257
Dll3	0.01850428
Dlx6os2	0.01505858
Dnaja1	0.02499043
Dnajb13	0.00177653
Dnajc28	0.02625527
Dnm3os	0.04143602
Dnmt3b	0.01597508
Doc2b	0.00015054
Dok4	0.00295490
Dpcr1	0.04585586
Dpysl5	0.03828625
Drp2	0.04694623
Dsc1	0.00690988
Dscaml1	0.00629671
Dusp16	0.00105510
Dusp2	0.03211343
E130215H24Rik	0.03919581
Ebf1	0.00664090
Ecd	0.00120214
Eci1	0.02143897
Edem2	0.02877674
Ednra	0.03904148
Eef2kmt	0.03927401
Efna1	0.00425318
Efna3	0.01016593

Egfl8	0.04845232
Eif3j1	0.00262565
Eif4e3	0.01285555
Eif4ebp1	0.02287248
Emb	0.01102159
Enpp1	0.04723923
Epha6	0.02099694
Ephx3	0.04449480
Erbb2ip	0.02641597
Ercc4	0.00438677
Erich1	0.02381118
Ermap	0.00254768
Esp34	0.00618891
Esp6	0.04889032
Espn	0.00348995
Etv2	0.02959118
Etv5	0.00093746
Exosc5	0.00023394
Eya4	0.03083309
F830016B08Rik	0.01980136
Fam101a	0.01396495
Fam104a	0.02189048
Fam110b	0.03830510
Fam111a	0.04449480
Fam131a	0.03559319
Fam155a	0.01693928
Fam188b	0.02769233
Fam196b	0.02445327
Fam198b	0.03651165
Fam19a1	0.02959443
Fam43b	0.00314711
Fam46a	0.03211343
Fam46b	0.02477176
Fam96b	0.03486888
Fbxo36	0.00905818
Fbxw20	0.03928315
Fbxw28	0.02883412
Fer1l4	0.00169442
Fetub	0.00640307
Fgfr1	0.04592880
Fgfr3	0.02769233
Fibcd1	0.02195558
Fkbp2	0.00049336
Flad1	0.02352948

Fmnl3	0.00263403
Fmo3	0.03679777
Foxa3	0.03559319
Foxb1	0.02994245
Foxo3	0.01025080
Foxred2	0.03312228
Foxs1	0.01975150
Fras1	0.01613505
Frmd3	0.01693928
Fsd2	0.02195558
Fshr	0.03075305
Ftcd	0.01261794
Furin	0.02161227
Fut8	0.00033151
Gab1	0.00585617
Galr2	0.02685617
Gchfr	0.00104565
Gcnt4	0.01285555
Gdf11	0.02287248
Gdf5	0.02018685
Gem	0.00851276
Gemin8	0.02555540
Gfra1	0.02842969
Gfra2	0.03150645
Glrx2	0.02842969
Glt28d2	0.02625527
Gm10634	0.03564442
Gm12888	0.04315608
Gm13031	0.00970370
Gm13089	0.01328123
Gm14085	0.02575428
Gm14124	0.00618891
Gm14164	0.04864488
Gm16387	0.04492528
Gm3317	0.01328123
Gm382	0.04889032
Gm527	0.02575428
Gm536	0.01505858
Gm5595	0.01648835
Gm6583	0.00425318
Gm6588	0.00499851
Gmfb	0.04447339
Gnai2	0.01809426
Gnaq	0.03904148

Gnaz	0.00802722
Gne	0.04054567
Gng7	0.01547264
Gnptab	0.01095964
Gp9	0.01505858
Gpc1	0.00816098
Gpd1l	0.04449480
Gpha2	0.01094245
Gpr150	0.03099809
Gpr158	0.02890545
Gpr35	0.00469941
Gpr39	0.04315608
Gprc5c	0.00013728
Gpt	0.01850428
Gpt2	0.00475465
Gramd4	0.01183101
Grasp	0.00022808
Grem1	0.02675881
Grik3	0.00295490
Grin2d	0.00544523
Grn	0.03919581
Gstm2	0.03486888
Gstt2	0.02877674
Gtdc1	0.02593827
Guca2a	0.00456050
Gucy2f	0.00950167
H2-M2	0.03441095
Harbi1	0.01777220
Haus7	0.01362100
Havcr2	0.00690988
Hdac5	0.04143602
Hesx1	0.02381118
Hexa	0.04845232
Hexim2	0.00355446
Hey1	0.02625527
Hist1h2bb	0.02959118
Hk1	0.04864488
Hnf1b	0.01922092
Hnrnpu	0.02287248
Hoxb2	0.03679777
Hoxb8	0.03679777
Hoxc13	0.04011481
Hpca	0.03211343
Hrh1	0.04295983

Hrk	0.02769233
Hs6st1	0.02161227
Hsd11b2	0.02381118
Hspb7	0.03441095
Htr5b	0.00201071
Hyal3	0.01197494
Hyal4	0.03679777
Ice1	0.02555540
Ift122	0.02842969
Ift81	0.01261794
Igfbp1	0.03441095
Igfbp7	0.02018685
Iigp1	0.03830510
Il1bos	0.04054567
Il23r	0.01850428
Ildr1	0.01613505
Ilvbl	0.04585586
Insl3	0.02685617
Ints8	0.03394980
Iqcg	0.01066491
Iqck	0.01353260
Itga11	0.04449480
Itgam	0.04492528
Itgb2l	0.04143602
Itgb7	0.01812491
Itih5	0.00519329
Itk	0.04865792
Itm2c	0.04723923
Jmy	0.03312228
Jph4	0.02898848
Kcnc3	0.02769233
Kcnip3	0.01498096
Kcnj12	0.01690706
Kcnk2	0.01952635
Kcnq1	0.03441095
Kctd10	0.04295983
Kctd14	0.00754002
Kctd9	0.03978764
Kdf1	0.02018685
Kif16bos	0.00104565
Kif5c	0.03275896
Kifc3	0.02575428
Klf5	0.01648835
Klhl13	0.02189048

Klhl17	0.03559319
Klhl23	0.00211785
Krt79	0.04845232
Krt9	0.03486888
Lamp3	0.00087048
Larp1b	0.02665236
Larp6	0.02195558
Lax1	0.02018685
Layn	0.01614018
Lcn10	0.00156943
Lenep	0.00618891
Lepr	0.00994634
Lgals12	0.00234035
Lgals9	0.02143897
Lhfpl4	0.03394980
Lima1	0.00712383
Limd1	0.01424618
Lin7a	0.02044872
Lmna	0.01025080
Lpcat2b	0.00666047
Lrrc2	0.00485993
Lrrc38	0.04183969
Lrrc57	0.04011481
Lrrc74b	0.02555540
Lrrn2	0.02106040
Lrtm2	0.01865191
Lsm4	0.01656024
Ltb4r1	0.01975150
Ltk	0.03075305
Ly6g6d	0.02685617
Ly96	0.04143602
Lysmd3	0.00295679
Mad2l2	0.03700644
Map10	0.00638522
Map3k13	0.01547264
Map3k9	0.04797764
Mapk1ip1	0.01505858
Mb21d2	0.00826840
Mcat	0.02990500
Mccc1os	0.04780030
Mcm8	0.02477176
Mcu	0.00577459
Mdm2	0.01922092
Med1	0.01189007

Med15	0.00595530
Mef2a	0.01952635
Megf10	0.02289127
Memo1	0.04011481
Metrnl	0.00153778
Mgme1	0.01225048
Micall1	0.00649639
Micu2	0.00355446
Mob2	0.04011481
Mocs1	0.00355446
Mocs2	0.00560699
Mog	0.00489743
Mogs	0.04606521
Mpnd	0.01362100
Mrpl27	0.03278409
Mrpl33	0.04104947
Mrps34	0.02685617
Msantd1	0.00231847
Msl3l2	0.04864488
Mtss1l	0.01754784
Murc	0.00253393
Mvb12b	0.00882142
Mvd	0.02318626
Mxd1	0.03686146
Mycl	0.00802928
Myd88	0.03802471
Myef2	0.03382926
Myl1	0.01396495
Myl10	0.04372614
Myrfl	0.03919581
Myzap	0.04864488
Mzf1	0.04492528
Ncoa1	0.01319346
Ncoa2	0.03087220
Ndufa4l2	0.04845232
Nedd1	0.01998370
Nell1	0.04183969
Neu2	0.04143602
Neurl1b	0.02161227
Nfasc	0.00536300
Nfat5	0.03682372
Ngef	0.02575428
Nme8	0.03486888
Nmnat2	0.01424618

Nmrk1	0.01498096
Nos1	0.04143602
Nphp3	0.01653362
Nr1i2	0.04183969
Nrxn2	0.01907660
Nsa2	0.04592880
Nsun3	0.03919581
Ntmt1	0.00104565
Ntn4	0.00544523
Nuak2	0.01142142
Nudc	0.01975150
Nudt18	0.04104947
Nufip2	0.00108562
Numbl	0.04723923
Nxnl2	0.01135205
Ocel1	0.00023394
Olfm2	0.00235687
Olfml2a	0.02499234
Olfml2b	0.02883412
Olfr1134	0.04889032
Olfr1443	0.01863437
Olfr325	0.04889032
Olfr329-ps	0.03928315
Olfr536	0.03919376
Olfr557	0.04889032
Olfr652	0.00051526
Onecut3	0.00108391
Opn1sw	0.01356929
Oscp1	0.00111579
Otulin	0.03919581
Oxct1	0.04295983
Oxct2a	0.01812491
P2rx6	0.03099809
P2rx7	0.03545622
P2ry13	0.02223941
P3h3	0.01197494
P4hb	0.03927401
Padi1	0.03211343
Paqr7	0.03802471
Parp1	0.03679777
Parp3	0.04585586
Pax2	0.03278409
Paxip1	0.01066491
Pdlim7	0.02287845

Pdss1	0.02555540
Peli2	0.01863437
Pfkfb3	0.01952635
Pfkl	0.02381118
Pfpl	0.04104947
Phactr1	0.04054365
Phactr4	0.03312228
Phf21a	0.03739224
Phf7	0.01933484
Phkb	0.00032030
Pi4kb	0.03679777
Pik3r1	0.01804983
Pinx1	0.02499234
Plac1	0.02499234
Plcb3	0.02195558
Plcl2	0.03441095
Pln	0.00536626
Plpp3	0.04054365
Pmaip1	0.04902307
Pnma2	0.00927802
Polh	0.02499234
Poln	0.03075305
Polr1d	0.03559319
Pou3f3	0.01037605
Pou4f1	0.02665236
Ppara	0.04393565
Ppcdc	0.01063142
Ppm1a	0.04902307
Ppm1h	0.04270838
Ppp1r14d	0.00023394
Ppp1r26	0.02419259
Ppp2r2d	0.00489743
Prdm13	0.02625527
Preb	0.00690988
Prelid1	0.00537788
Primpol	0.02842969
Prkd2	0.01197494
Prl3d3	0.04889032
Prrc2c	0.03830510
Prss22	0.04143602
Prss44	0.02675881
Psmb8	0.00301512
Psmc3	0.00127532
Psmd9	0.01063142

Psme1	0.01362100
Ptchd4	0.02575428
Pus7	0.02842969
Pycard	0.00638522
Pygm	0.02143897
Qser1	0.00462941
R3hdm4	0.02990500
Rab11fip1	0.02553595
Rab24	0.02990500
Rab40c	0.02842969
Rad54l	0.00425318
Ralgapa2	0.01075710
Rangrf	0.03700644
Rasa1	0.04723923
Rassf6	0.02778541
Rbck1	0.01690706
Rbm12	0.03211343
Rbm4	0.04780030
Rbx1	0.01025080
Rcsd1	0.01754784
Rcvrn	0.03075305
Rd3	0.04315608
Rdh19	0.03802471
Reg4	0.00396185
Rem2	0.00022808
Rep15	0.00544523
Rfx7	0.01632042
Rgs19	0.03099809
Rhbdl2	0.04183969
Rhobtb1	0.03686146
Rhoh	0.00954406
Rilpl1	0.02990500
Rims2	0.01362100
Rnase2a	0.03325104
Rnasel	0.00779533
Rnf149	0.01597508
Rnf183	0.00754002
Rnf224	0.01754784
Rnf40	0.04449480
Rnft2	0.00224822
Romo1	0.00177653
Rpap2	0.02769233
Rpp25l	0.01975150
Rps19bp1	0.00905818

Rras2	0.01653362
Rrm2b	0.02780302
Rs1	0.01735212
Rsrc1	0.02890545
Rsrp1	0.03150645
Rtp3	0.03441095
Rxra	0.04183969
S100a11	0.01812491
S100b	0.00960236
Saal1	0.02140204
Sbk1	0.04797764
Sbno2	0.00284482
Scn3b	0.01241930
Sec14l1	0.01804983
Sec24c	0.04592880
Sema4b	0.03830510
Sema6b	0.01933484
Senp1	0.01189007
Senp8	0.03312228
Serinc3	0.00851276
Serpinb6a	0.02625527
Serpinb6c	0.01094245
Sftpb	0.04606521
Sh3rf1	0.01353260
Sh3rf3	0.03830510
Shisa8	0.00456050
Shroom1	0.00779533
Sla	0.03071801
Slain2	0.03545622
Slc10a6	0.01267995
Slc22a17	0.04449480
Slc22a22	0.00707139
Slc24a2	0.02608991
Slc25a17	0.02099694
Slc25a18	0.00853320
Slc28a2	0.02990500
Slc29a3	0.00106367
Slc29a4	0.01614018
Slc2a6	0.00951772
Slc2a9	0.02842969
Slc35b3	0.04864488
Slc35d2	0.03919376
Slc35g3	0.00463624
Slc43a3	0.00225411

Slc44a3	0.01850428
Slc47a1	0.01547264
Slc4a4	0.00182278
Slitrk5	0.02898848
Smc1b	0.03278409
Smo	0.00138424
Smpd4	0.00666047
Snapin	0.00044253
Snx31	0.00502454
Snx6	0.01142142
Sowahd	0.02106040
Sox10	0.02018685
Sox14	0.03486888
Sp100	0.01701257
Spast	0.00848678
Spc24	0.02018685
Speg	0.04902307
Spem1	0.04889032
Spg21	0.01922092
Spink6	0.00499851
Sprn	0.03312228
Sprr1a	0.02685617
Sprr2a2	0.02018685
Srrm4	0.04902307
Srsf12	0.01252403
Ssh3	0.02990500
St3gal2	0.00128401
St3gal5	0.03927401
St6galnac1	0.02990500
St6galnac4	0.03828625
St8sia1	0.03828625
Stat5a	0.02842969
Strip2	0.03275896
Stt3b	0.02994245
Swsap1	0.02675881
Syce1	0.00060616
Sync	0.02287845
Syt15	0.01353781
Tal1	0.03739224
Taok1	0.04054365
Taok2	0.01809426
Tars2	0.04393565
Tax1bp3	0.02352948
Tbc1d31	0.04130955

Tbcd	0.02877674
Tcea1	0.00087048
Tceb3	0.01653362
Tcfl5	0.02769233
Tecpr1	0.03211343
Tex16	0.04585586
Thnsl2	0.04372614
Thrb	0.02917970
Thyn1	0.01539429
Tiam1	0.02364762
Timd2	0.01597508
Timm8a1	0.01809426
Tln2	0.03651165
Tlr5	0.03075305
Tm4sf19	0.00456050
Tmco1	0.04492528
Tmem107	0.02018685
Tmem132c	0.02039334
Tmem151b	0.00670075
Tmem158	0.03441095
Tmem243	0.01754784
Tmem26	0.00218513
Tmem263	0.01163213
Tmem30b	0.03739224
Tmem38a	0.04864488
Tmem39b	0.00577459
Tmem67	0.04611623
Tmem70	0.00128401
Tmprss13	0.01809426
Tmtc4	0.01461033
Tnfrsf12a	0.02477176
Tnrc6b	0.01055039
Tns3	0.03341928
Toe1	0.00282878
Tor1aip1	0.00019862
Tor1aip2	0.02788922
Tpm2	0.02994245
Trabd2b	0.01449990
Trappc9	0.00514656
Treml4	0.00816098
Trim12a	0.00723546
Trim61	0.02143897
Trmt44	0.03927401
Trp53i11	0.00585860

Tspan14	0.03150645
Tspan18	0.00395578
Ttc23	0.01285555
Tubb4a	0.00010906
Tubb6	0.00537788
Txk	0.00901750
Txnl4a	0.01241930
Ubald1	0.01850428
Ube2c	0.00201071
Ube2cbp	0.03325104
Ubr7	0.03394980
Uhrf1bp1l	0.00732646
Unc93a	0.02099694
Uncx	0.04054567
Unk	0.02842969
Upf3b	0.02625527
Upk2	0.03486888
Usp13	0.00054494
Usp25	0.00558184
Usp29	0.04054365
Usp32	0.02340376
Vamp1	0.02140204
Vamp5	0.00368464
Vav3	0.03904148
Vill	0.03919581
Vimp	0.02287248
Vmn2r88	0.04295983
Vps13b	0.03156866
Vps25	0.00916503
Vps35	0.04295983
Vps72	0.01362100
Wbp1	0.00231847
Wdr46	0.00662110
Wdr48	0.03341928
Wdr53	0.02959118
Whrn	0.04449480
Wnk1	0.02320865
Wnt10a	0.00147098
Xirp1	0.00848678
Xrcc3	0.04449480
Yae1d1	0.04592880
Zak	0.01599046
Zbtb2	0.04104947
Zbtb32	0.00970370

Zbtb34	0.01472184
Zc3h7b	0.02445327
Zcchc11	0.04952602
Zcchc24	0.00848678
Zcchc4	0.01693928
Zdhhc17	0.03830510
Zfhx2	0.00074915
Zfp108	0.00006000
Zfp236	0.04104947
Zfp263	0.04585586
Zfp352	0.01328123
Zfp385a	0.04723923
Zfp428	0.01656024
Zfp433	0.00038148
Zfp46	0.02780302
Zfp488	0.03394980
Zfp516	0.00886401
Zfp609	0.02287248
Zfp641	0.00205223
Zfp663	0.00087361
Zfp746	0.03739224
Zfp78	0.00059093
Zfp862-ps	0.01505858
Zfp959	0.00049336
Zfyve27	0.02223941
Zhx3	0.00342778
Zmym3	0.01653362
Zmynd15	0.01466926
Znrf2	0.01388870
Zswim1	0.00385831

Supplementary Fig. 4

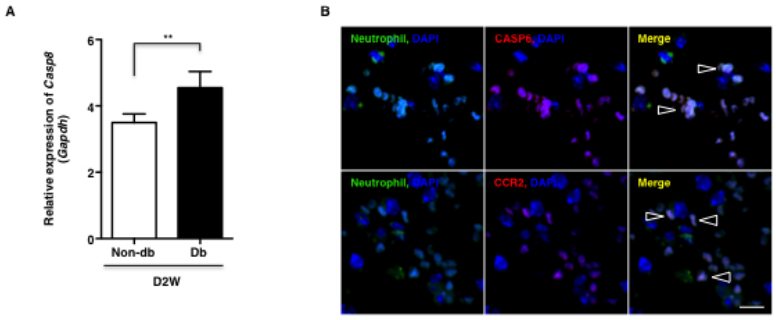

254x190mm (72 x 72 DPI)

Supplementary Fig. 5

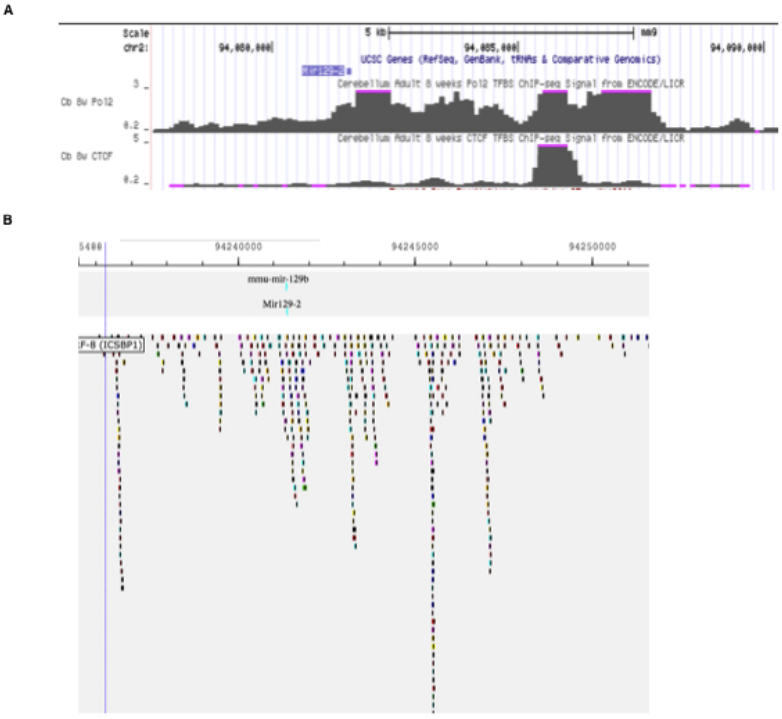

254x190mm (72 x 72 DPI)